GSICS Impact on MTP Products

Doc.No. : EUM/RSP/REP/14/783586
Issue : v2A e-signed
Date : 19 February 2016
WBS/DBS :

EUMETSAT
Eumetsat-Allee 1, D-64295 Darmstadt, Germany
Tel: +49 6151 807-7
Fax: +49 6151 807 555
http://www.eumetsat.int

This page intentionally left blank.

Document Change Record

Issue / Revision	*Date*	*DCN. No*	*Changed Pages / Paragraphs*
1	5 February 2016		Initial Issue of document.
2	12 February 2016		First team review of document version.
2A	19 February 29016		Final review and publishing of document.

Table of Contents

Table of Figures

1 INTRODUCTION

1.0 Purpose

Inter-calibration products between Meteosat-7 MVIRI and Metop-A IASI as proposed by the Global Space Based Inter-Calibration System (GSICS) show that for "standard radiances" (typical of clear sky scenes in the sub-tropics) Meteosat 7 Water Vapour (WV) channel is ~2.6 K too warm, and the Infra red (IR) channel is ~3.2 K too cold compared to Infrared Atmospheric Sounding Interferometer (IASI). There is currently no bias corrections applied to Meteosat 7 counts/radiance in the EUMETSAT operational processing. However, such large biases may have a severe impact on the outputs or the quality of Meteorological Products extracted from Meteosat 7 imagery.

This report contains research and analysis of the impact of applying GSICS calibration coefficients on Meteosat First Generation (MFG) Meteorological Products extracted at MTP MPEF. The following MFG products have been compared during a period of five days (15 to 20 October 2014):

Identifier	*Product Name*
CLA	Cloud Analysis
CLM	Cloud Mask
CSR	Clear Sky Radiance
CTH	Cloud Top Height
ELW	Expanded low-resolution cloud motion winds
HRV	High resolution visible winds
HWW	High resolution water vapour winds
WVW	Clear sky water vapour winds

1.1 Document Structure

No.	Section Name	Description
1	Introduction	This introduction
2	Definitions and Abbreviations	This section describes verification activities concerning comparisons done in this study.
3	Data Preparation	Detailed results with respect to data preparation
4	Detailed Results	Detailed results with respect to impact of GSICS correction on every MTP product
6	Conclusions	Conclusions of the study

1.2 Applicable Documents

Ref	Title	EUMETSAT Reference
RD 1	'ReadMe for GSICS Demo NRT Correction of MVIRI-IASI	EUM/MET/DOC/11/0396

2 DEFINITIONS AND ABBREVIATIONS

This section contains all definitions and abbreviations that are not included in the MSG SYSTEM Glossary of Terms and List of Acronyms. Also, the validation strategy and some findings during the validation period are discussed.

2.0 Additional acronyms used in this document

Acronym	*Meaning*
CLA	Cloud Analysis
CLM	Cloud Mask
CSR	Clear Sky Radiance
CTH	Cloud Top Height
ELW	Expanded low-resolution cloud motion winds
HRV	High resolution visible winds
HWW	High resolution water vapour winds
WVW	Clear sky water vapour winds

2.1 Definitions used in this document

Within this document, references are made to the following terms. The table below provides a short description of the meaning as used in the descriptions and specifications in this document.

Term	*Specification*
Low-level clouds	Clouds with a height assignment between the Surface and 700 hPa.
Medium-level clouds	Clouds with a height assignment between 700 and 400 hPa.
High-level clouds	Clouds with a height assignment above 700 hPa.

2.2 Comparison Strategy

The comparison was done between the product outputs from MFG MPEF chain, and product outputs tested on VAL MPEF. GSICS corrections have been implemented on VAL MPEF, while the OPE chain remained uncorrected. Due to system restrictions, the comparison period is limited to five days, 15 to 20 October 2014. However, the results below show that such 5 days period is enough to get a good estimation of the impact of applying GSICS coefficient on MFG product retrieval.

Various kinds of plots illustrate such impact below. Examples of OPE product together with OPE-VAL product differences are plotted on an MFG disk. However, histograms and time series are also considered, to give an idea of the size of the magnitude of the impact.

3 DATA PREPARATION

The methodology to apply the Meteosat/MVIRI cross-calibration against IASI on the MTP MPEF system consists of modifying the original calibration coefficients for the count-to-radiance conversion. The advantage of this method is that all the MPEF algorithms access the calibration coefficients via a common function. Implementing the changes inside this function ensures that all algorithms will run with the converted radiances.

This conversion is performed as follows:

$$L = gain \times (Image\_count - space\_count)$$

Our goal is to determine $gain_c$ and $space\_count_c$ so that the corrected radiance is expressed as follows:

$$L_c = gain_c \times (Image\_count - space\_count_c)$$

The cross-calibration method for Meteosat/MVIRI and IASI is derived in [*RD 1*]:

From the equations detailed in this document, we can derive the formula to modify the MTP MPEF calibration coefficients in order to match the IASI reference:

$$gain_c = \frac{gain}{b_r}$$

$$space\_count_c = space\_count + \frac{a_r}{gain} \times \frac{filter\_integral}{1000}$$

Where a_r and b_r are respectively the offset and the gain provided by the GSICS products and *filter_integral/1000* is the conversion factor from spectral to broadband radiances for MVIRI.

The data for the experiment were extracted from the GSICS MET-7/IASI product for the 6 August 2014[1]. The actual numerical values for the corrected calibration are the following:

WV channel:	**IR channel:**
$gain_c = \frac{gain}{1.101982}$	$gain_c = \frac{gain}{0.9303573}$
$space\_count_c = space\_count - \frac{0.00539}{gain}$	$space\_count_c = space\_count + \frac{0.34396}{gain}$

[1] The data collection started in August 2014, but unfortunately only the period 15 - 20 October was properly saved and usable for this analysis. Not considering Near Real Time GSICS correction may create important discrepancies on the results because the instrument's calibration can vary with time. However, a quick check on GSICS Bias Monitoring plots (http://tcweb.eumetsat.int/tcc1/proj/gsics/web/BiasMonitoring.html) reveals only relatively small changes (<10% of the bias) over this interval.

4 DETAILED RESULTS

4.1 Comparison of CLM product

4.1.1 Objective

The Cloud Mask (CLM) product is an image-based GRIB Edition 2 encoded product which indicates the presence of clouds. The CLM product is derived from an internal classification image product, which is based on pixel-based cloud analysis retrieval. Within the encoding of the product, the pixels are identified as follows:

- Cloudy
- Clear Sky over Land
- Clear Sky over Sea
- Not identified

This product is used in many of the other algorithms that extract Meteorological Products from MFG, like CLA, CSR, or wind vectors.

4.1.2 Summary

As expected, the impact of GSICS calibration coefficients on the cloud mask is very large. It mainly impacts the amount of cloudy pixels identified in the image, which is nearly 20 % larger on OPE than on VAL chain. This is due to thresholding methods used to flag the scenes from MFG imagery.
The cloud mask is used further for the estimation of other products like winds or CLA. Using a very different cloud mask on VAL is expected to impact further the retrieval of the other algorithms that use the cloud mask as input.

4.1.3 Visualisation of the product

The top panel in Figure 1 shows an example of CLM product obtained on OPE (left) and VAL (right) chains on 18 October 2014 at 12:30 UTC. There are many more pixels identified as cloudy pixels (white patterns) on OPE chain than on the VAL chain.

Time series of cloud amount over the five days plotted on the middle panel shows a small diurnal cycle, and a systematically larger amount of cloudy pixels (75 %) on OPE chain than on VAL chain (55%).

Bottom plot illustrates the histograms of Clear sky Ocean (value 0), cloudy (value 1) and clear sky land (value 2) pixel identifications.

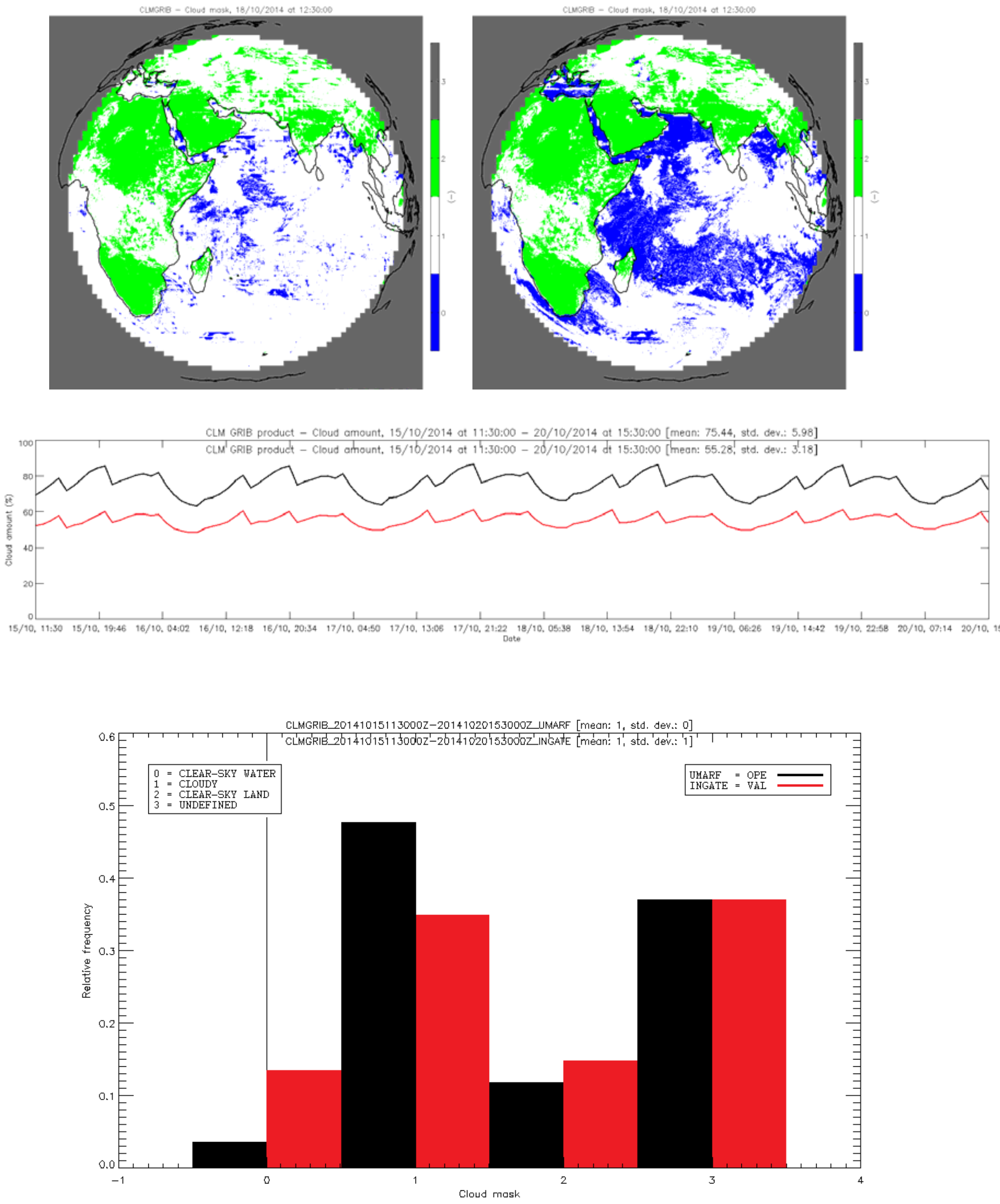

Figure 1: Example of CLM product obtained on OPE (Top left) and the difference OPE-VAL (Top right) on 18 October 2014 at 12:30 UTC. Corresponding time series of cloud amounts (middle) and histograms of CLM scenes (bottom) over the period are also presented.

.

4.2 Comparison of CLA product

4.2.1 Objective

The Cloud Analysis (CLA) provides information on cloud type, cloud top height and cloud top temperature on a pixel basis. The CLA algorithm uses CLM product as input to estimate the cloud parameters only for the cloudy pixels.

However, the CLA product obtained on the OPE chain is not stored on a pixel basis, but is an average of the CLA pixel-based information over a 32 × 32 pixels segments. In this section, the Cloud Top temperature and Cloud top pressure averaged over these segments are compared against the ones obtained on the VAL chain.

A cloud amount, which represents the rate of the cloudy pixels over the segment, is also stored in the product and has been compared for OPE and VAL.

4.2.2 Summary

The average Cloud amount is smaller on the VAL chain (30 %) than on the OPE chain (41 %). This is directly linked to the difference noted on the CLM product, where 20 % more pixels are identified as cloudy on OPE chain. The two histograms of cloud amount are quite similar for OPE and VAL, but the peak at 10 – 20 % is more pronounced for results obtained on the VAL chain. On the opposite end, the amount of segment totally cloudy (100 % cloud amount) is logically much larger on the OPE chain.

Results regarding the Cloud top pressure and Cloud top temperature are similar for the OPE and VAL chains. Mean cloud top temperatures are equal to 267 K (OPE) and 262.5 K (VAL). This results in slightly higher mean cloud top altitude (564 hPa) on VAL than on OPE (597 hPa). The respective histograms shown in Figure 3 and Figure 4 show similar distributions of the cloud top temperature and cloud top pressure on OPE and on VAL chains over the period. However, more clouds are found at slightly higher altitude on VAL chain in comparison to OPE.

It must be noted that all these results on CLA product must be considered very carefully as they contained information that are averaged over a segment, and not extracted on a pixel basis. Therefore it is difficult to estimate the impact of the averaging process on the results, accounting that very large heterogeneity of situation may coexist within the segments.

4.2.3 Visualisation of the product

The top of Figure 2 shows an example of Cloud amount parameter from CLA product obtained on OPE (left) and the difference OPE-VAL (right) 18 October 2014 at 14:02 UTC.

Time series of cloud amount over the five days is plotted on the middle panel. Dashed lines represent the minimum and maximum values.

The bottom plot illustrates the relative histograms of cloud amounts from OPE (black) and VAL (red) chains.

Figure 3 is similar to Figure 2 but for the Cloud top temperature parameter of the CLA product.
Figure 4 is similar to Figure 2 but for the Cloud top Pressure parameter of CLA product.

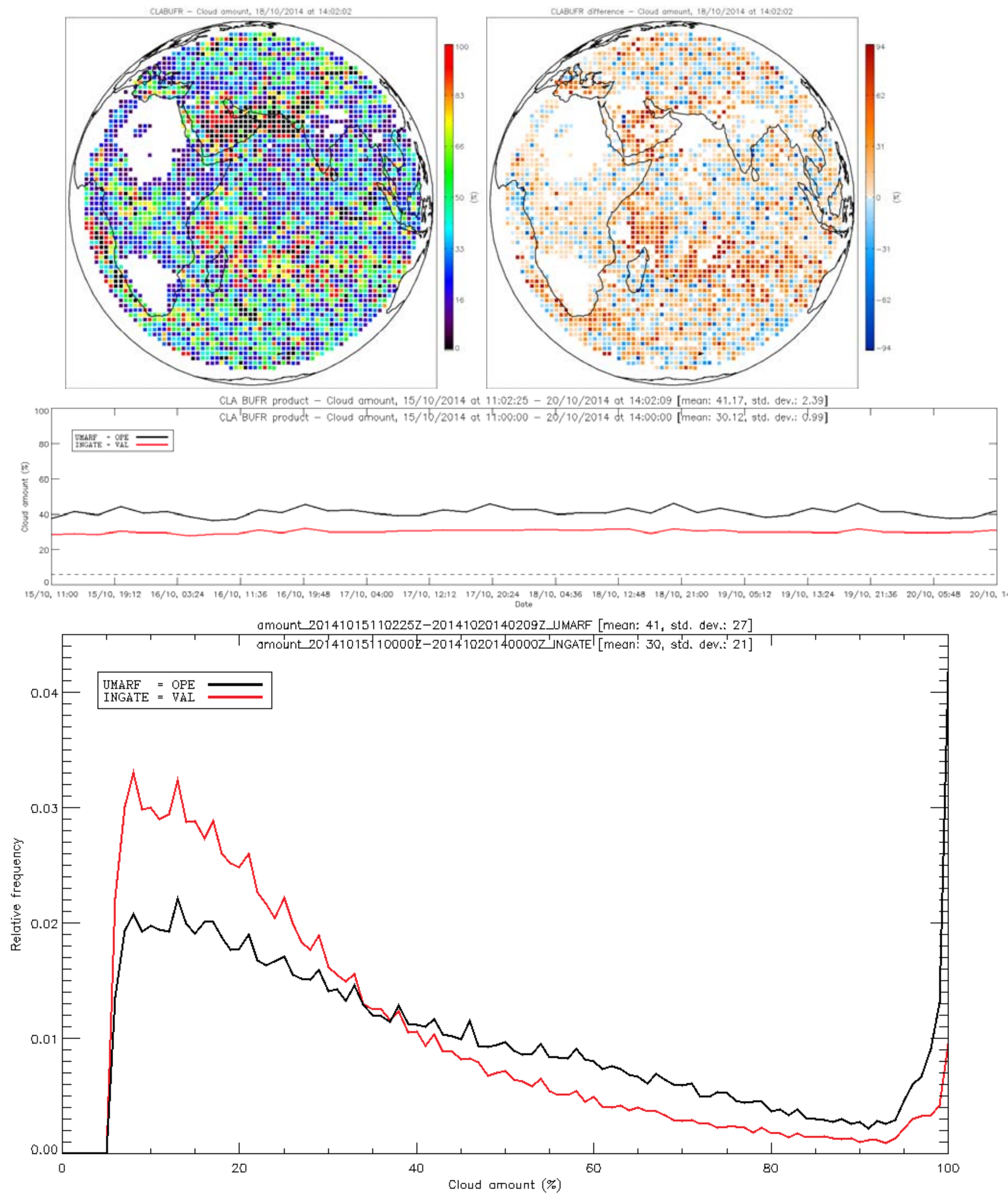

Figure 2: Cloud amount parameter of CLA product obtained on OPE (top left) and the difference OPE-VAL (top right) on 18 October 2014 at 14:02 UTC. Corresponding time series (middle) and histograms (bottom) of this parameter over the period are also presented.

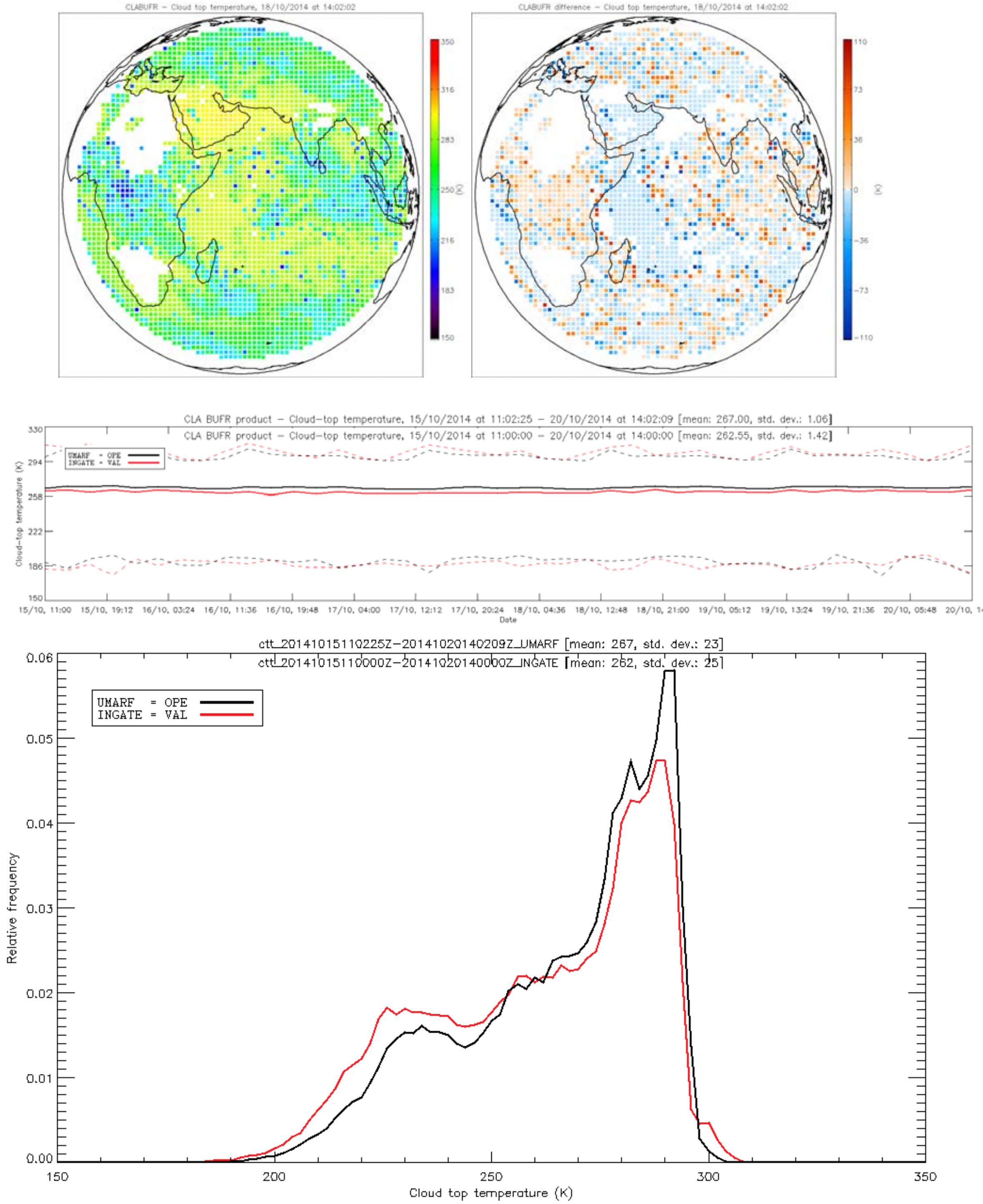

Figure 3: Cloud top temperature parameter of CLA product obtained on OPE (top left) and the difference OPE-VAL (top right) on 18 October 2014 at 14:02 UTC. Corresponding time series (middle) and histograms (bottom) of this parameter over the period are also presented.

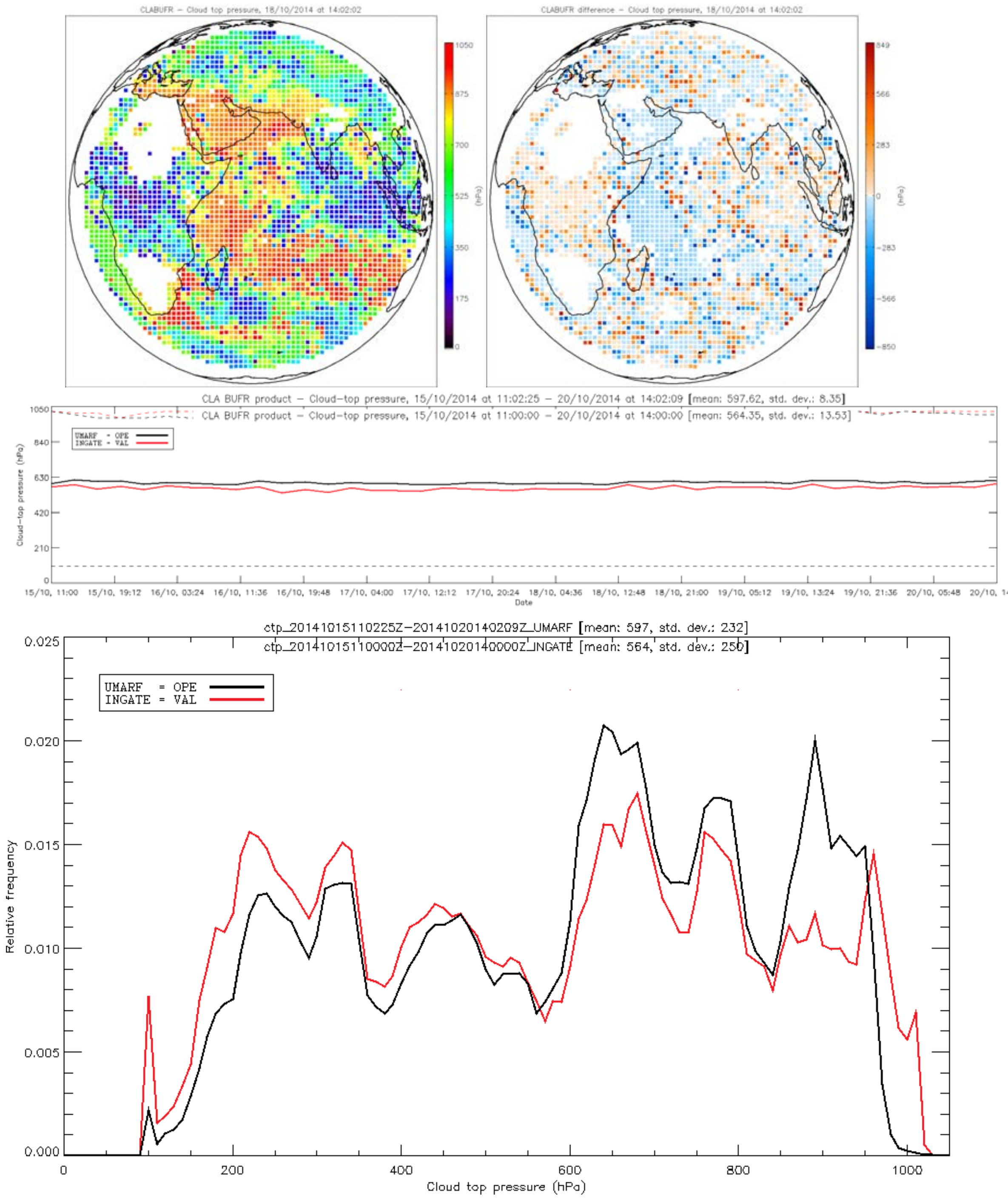

Figure 4: Cloud top pressure parameter of CLA product obtained on OPE (top left) and the difference OPE-VAL (top right) on 18 October 2014 at 14:02 UTC. Corresponding time series (middle) and histograms (bottom) of this parameter over the period are also presented.

4.3 Comparison of CSR product

4.3.1 Objective

The Clear Sky Radiances (CSR) product contains information on mean brightness temperatures and radiances from all thermal (e.g. water vapour and infrared) channels averaged over 16x16 pixels segments. Information on the cloud free amount and cloud amount is also stored in the output file. The CSR is derived every hour.

4.3.2 Summary

The differences between the cloud amount and cloud-free amount on OPE and VAL chains are very similar. The cloud-free amount is a bit larger and the cloud amount a bit smaller on VAL chain. This is probably due to the impact of the cloud mask on the averaging over the segment. The histograms of cloud free amount and cloud amount are similar.

A bias around 2.9 K exists between the brightness temperatures extracted from OPE and VAL for the water vapour channel and around –1.5 K for infrared channel. Obviously, this directly corresponds to the GSICS correction applied on the counts to radiance conversion on VAL chain. This is smaller than the “standard bias” derived from the GSICS Correction, because the bias is smaller for colder scenes.

4.3.3 Visualisation of the product

The top panel in Figure 5 shows an example of the cloud-free amount parameter from the CSR product obtained on OPE (left) and the difference OPE-VAL (right) on 18 October 2014 at 12:02 UTC for the water vapour 6.2 channel.

Time series and histograms of cloud free amount obtained on OPE and VAL chains over the five days are plotted on the middle and bottom panels respectively. You will notice the following comparisons:

- Figure 6 is similar to Figure 5 save for the cloud amount of CSR product.
- Figure 7 is similar to Figure 5 save for the brightness temperature parameter of the CSR product.
- Figure 8 is similar to Figure 7 save for the Radiance parameter of the CSR product.
- Figures 9, Figure 10, Figure 11 and Figure 12 are similar to Figure 5, Figure 6, Figure 7 and Figure 8 respectively, except for the infrared 10.8 channel.

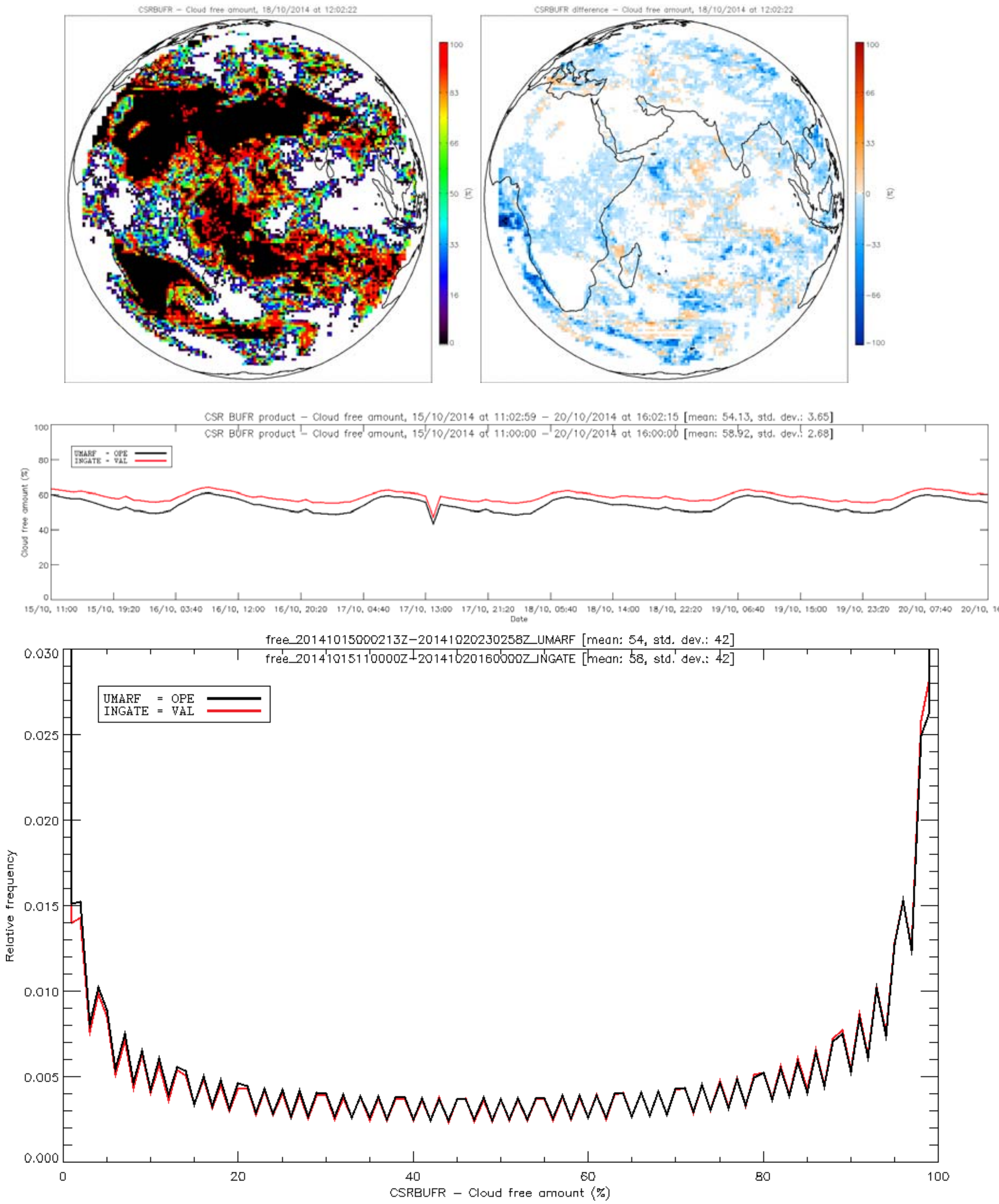

Figure 5: Cloud-free amount parameter of CSR product obtained on OPE (top left) and the difference OPE-VAL (top right) on 18 October 2014 at 12:02 UTC. Corresponding time series (middle) and histograms (bottom) of this parameter over the period are also presented. Water Vapour 6.2 channel.

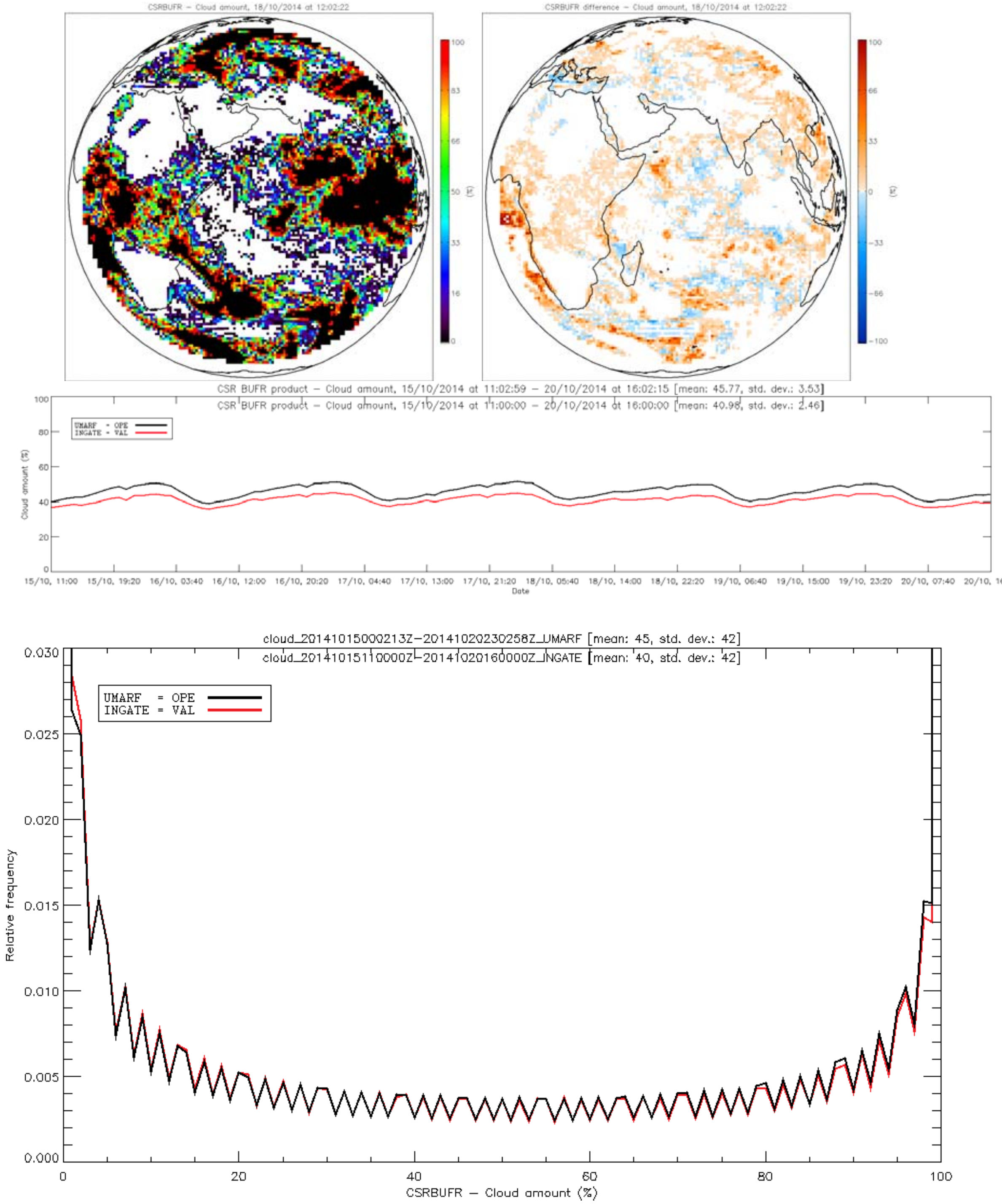

Figure 6: Cloud amount parameter of CSR product obtained on OPE (top left) and the difference OPE-VAL (top right) on 18 October 2014 at 12:02 UTC. Corresponding time series (middle) and histograms (bottom) of this parameter over the period are also presented. Water Vapour 6.2 channel.

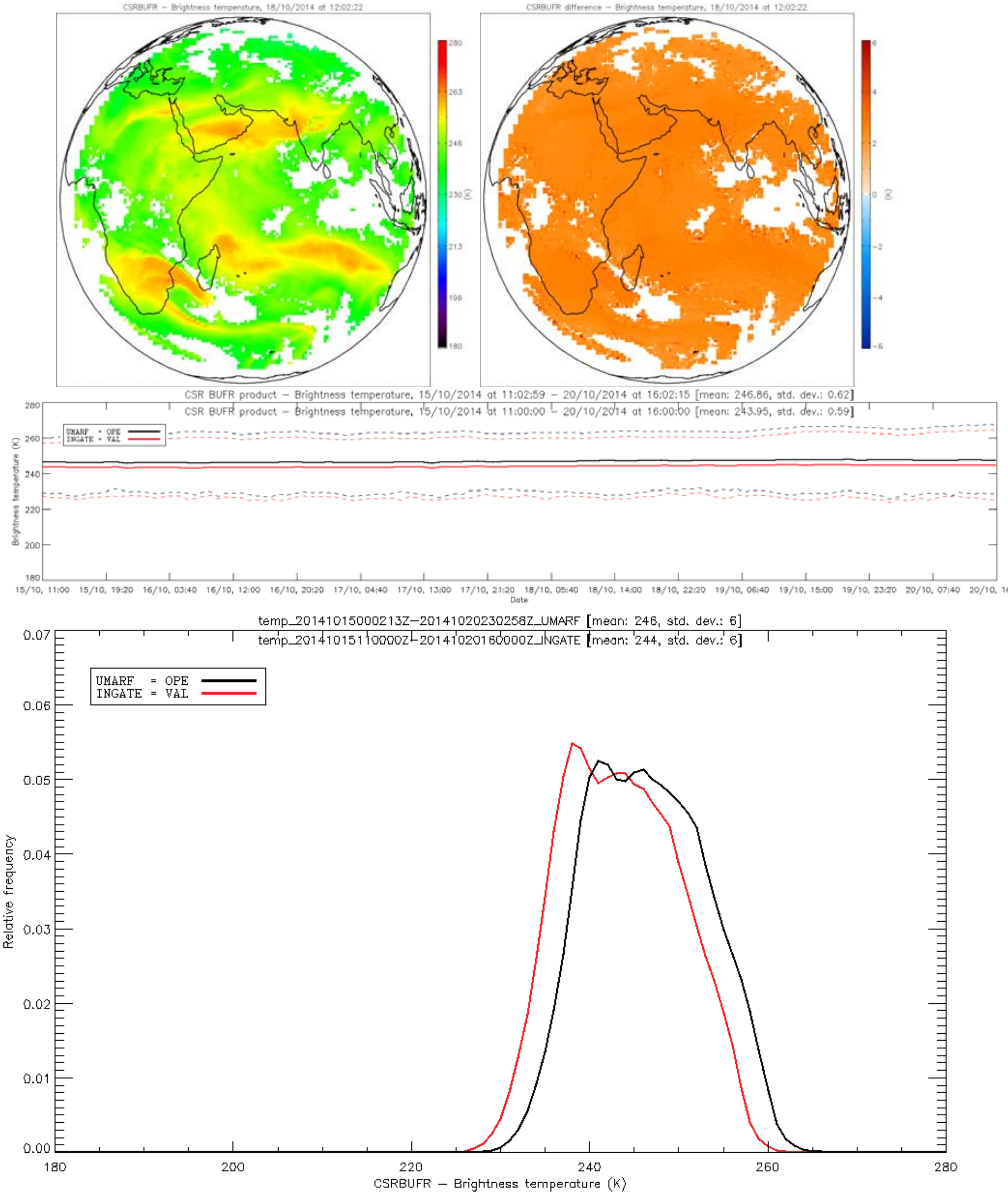

Figure 7: Brightness temperature parameter of CSR product obtained on OPE (rop left) and the difference OPE-VAL (top right) on 18 October 2014 at 12:02 UTC. Corresponding time series (middle) and histograms (bottom) of this parameter over the period are also presented. Water Vapour 6.2 channel.

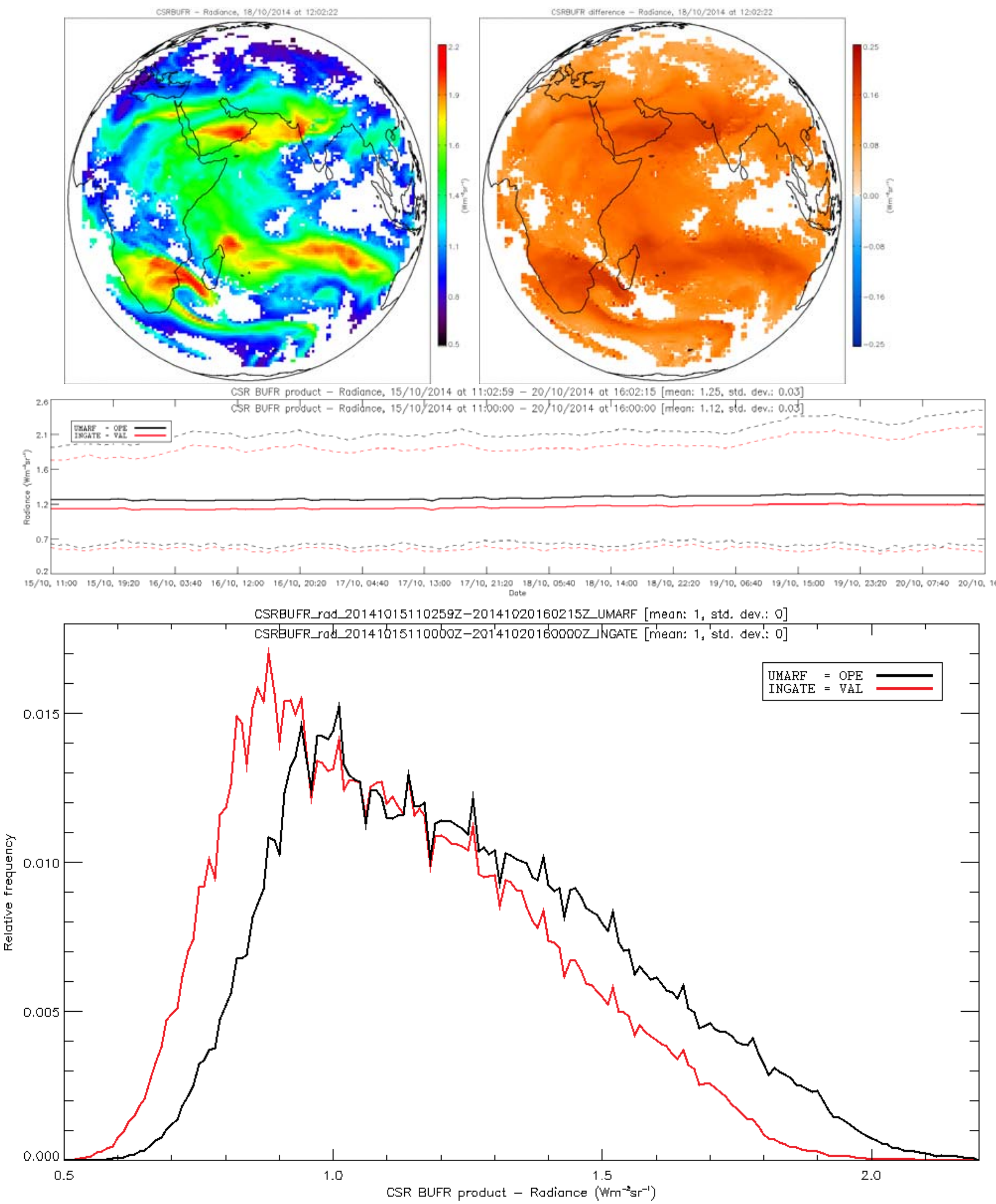

Figure 8: Radiance parameter of CSR product obtained on OPE (Top left) and the difference OPE-VAL (Top right) on 18 October 2014 at 12:02 UTC. Corresponding time series (middle) and histograms (bottom) of this parameter over the period are also presented. Water Vapour 6.2 channel.

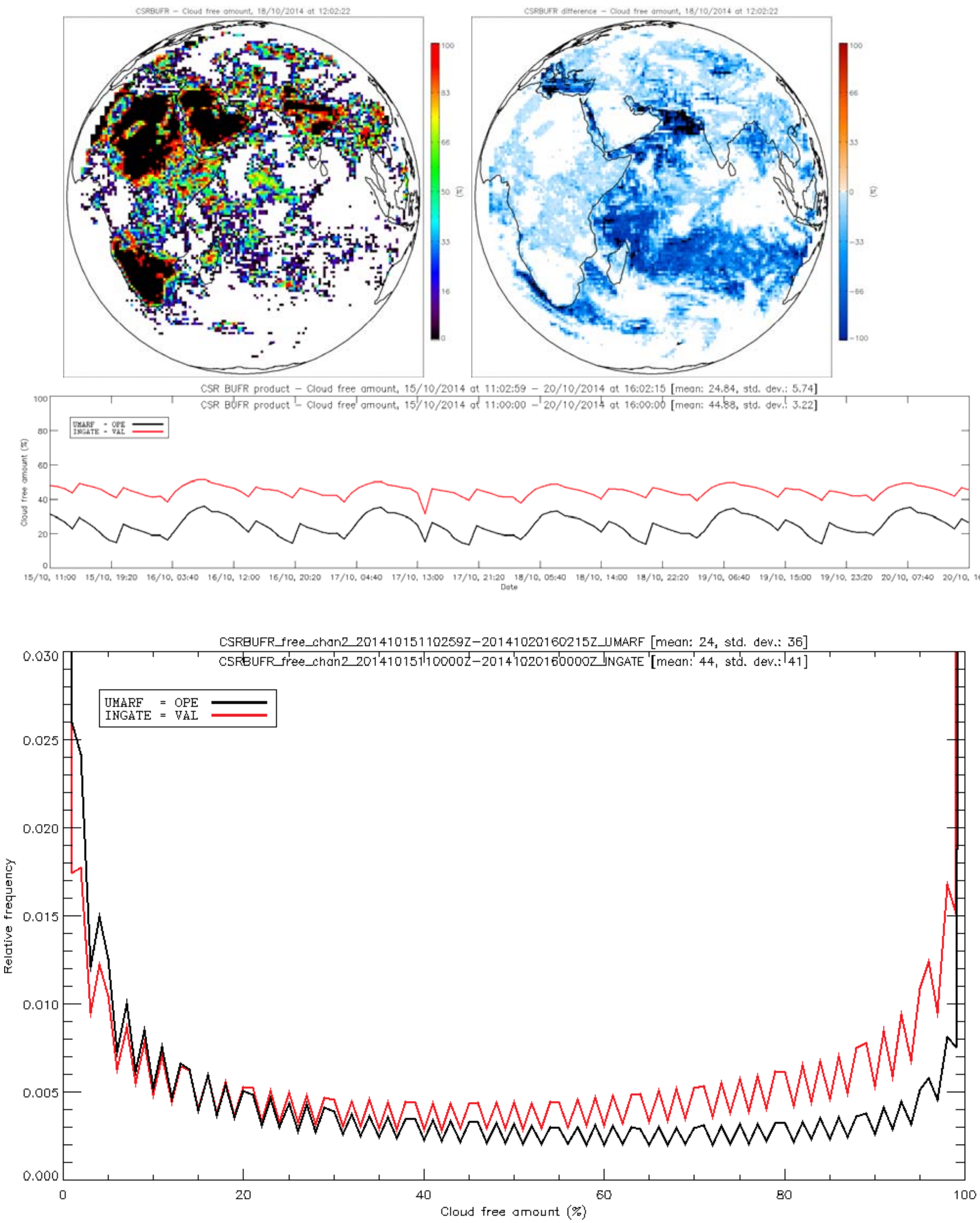

Figure 9: Cloud-free amount parameter of CSR product obtained on OPE (Top left) and the difference OPE-VAL (Top right) on 18 October 2014 at 12:02 UTC. Corresponding time series (middle) and histograms (bottom) of this parameter over the period are also presented. Infrared 10.8 channel.

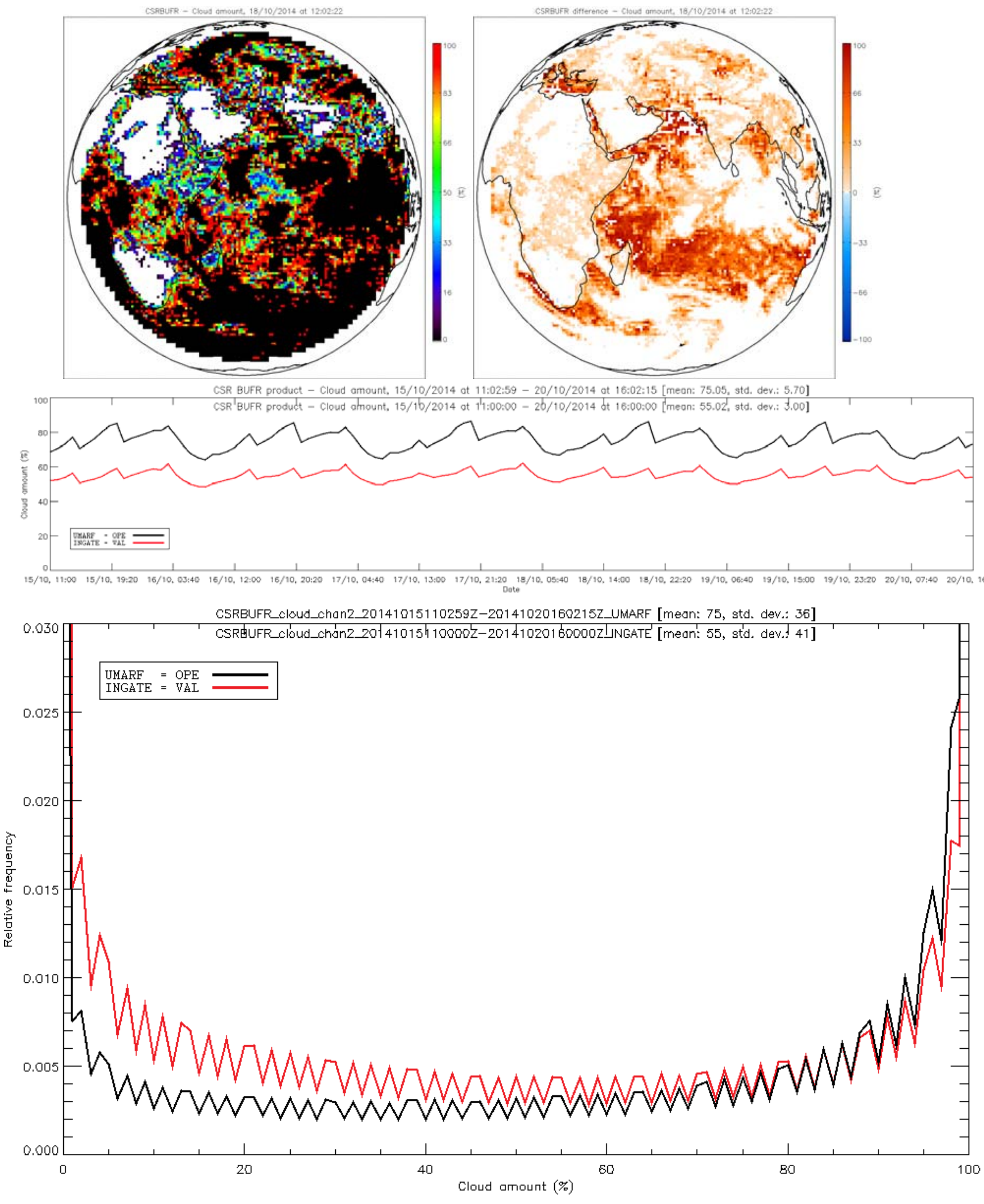

Figure 10: Cloud amount parameter of CSR product obtained on OPE (top left) and the difference OPE-VAL (top right) on 18 October 2014 at 12:02 UTC. Corresponding time series (middle) and histograms (bottom) of this parameter over the period are also presented. Infrared 10.8 channel.

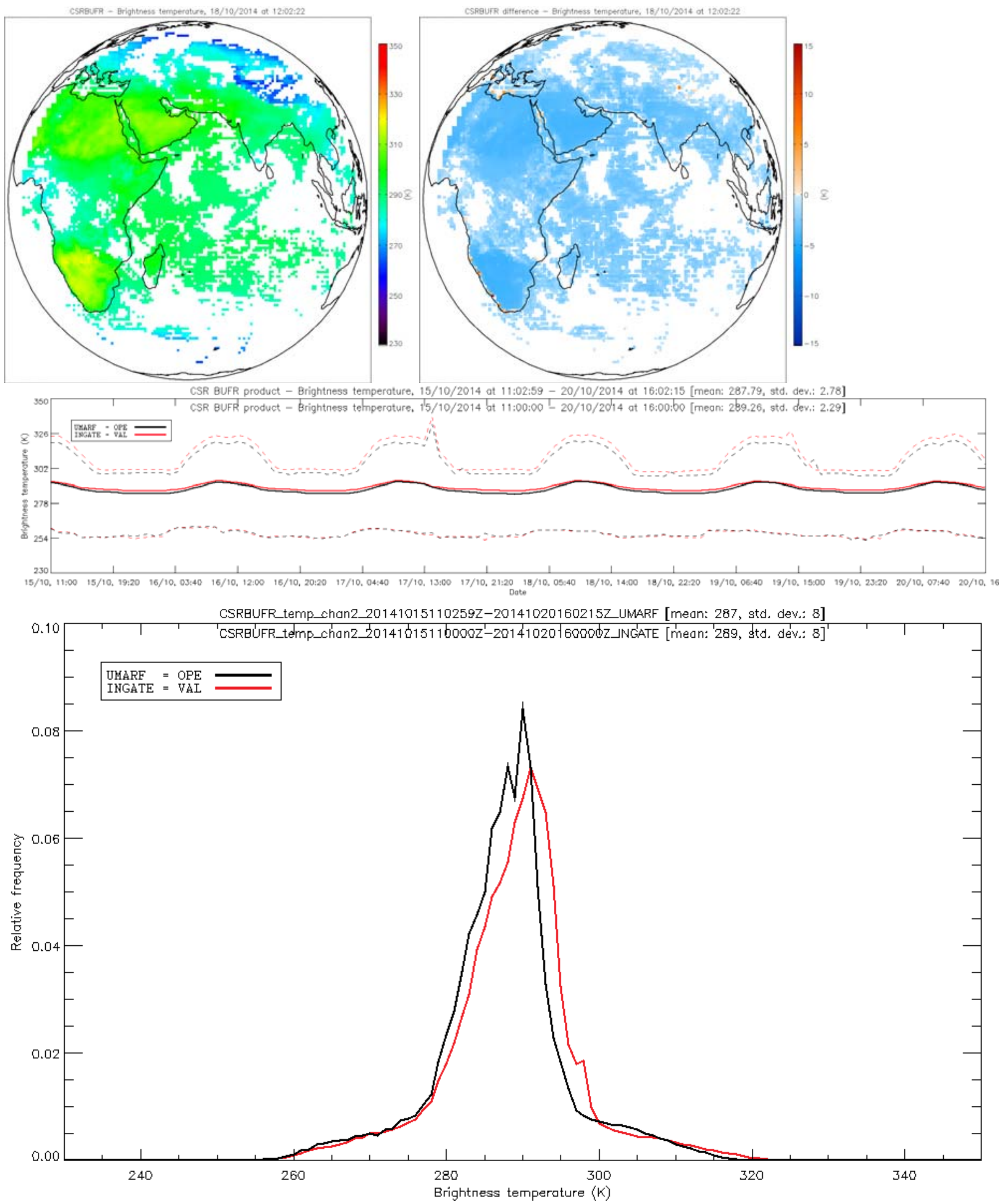

Figure 11: Brightness temperature parameter of CSR product obtained on OPE (top left) and the difference OPE-VAL (top right) on 18 October 2014 at 12:02 UTC. Corresponding time series (middle) and histograms (bottom) of this parameter over the period are also presented. Infrared 10.8 channel.

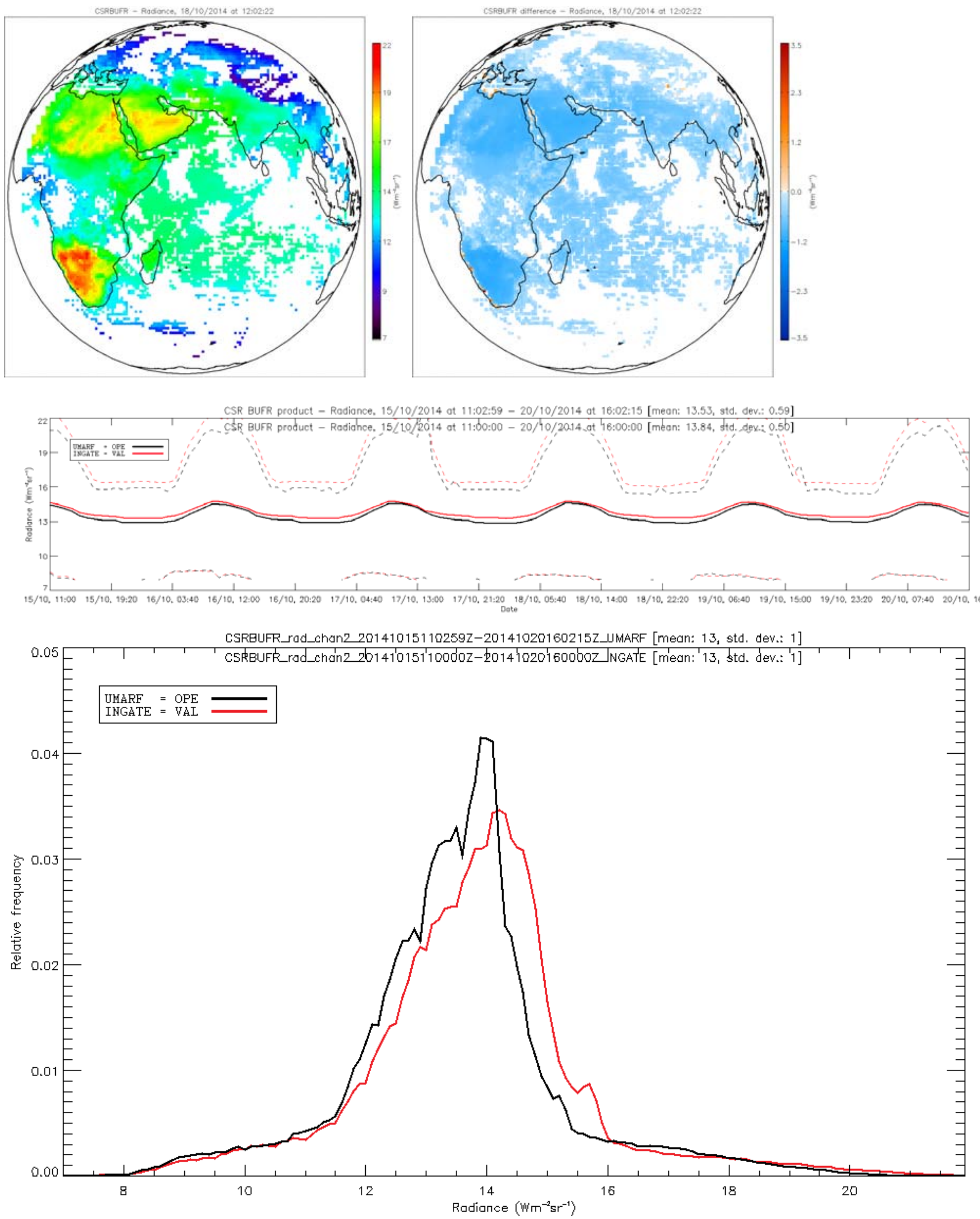

Figure 12: Radiance parameter of CSR product obtained on OPE (top left) and the difference OPE-VAL (top right) on 18 October 2014 at 12:02 UTC. Corresponding time series (middle) and histograms (bottom) of this parameter over the period are also presented. Infrared 10.8 channel.

4.4 Comparison of Expanded Low-resolution Winds (ELW)

4.4.1 Objective

This product was introduced in 1996 as an alternative to the SATOB (satellite cloud drift winds) product, which contained all winds from all three channels and used the low resolution 80 × 80 segment matrix. Since 2 December 2002, the ELW product has used only winds from the IR. As a replacement for the low-resolution VIS and WV AMVs (as a SATOB-coded product), we encourage users to use the HRV and HWW instead. The ELW product is generated every 1.5 hours and distributed in BUFR code. A typical ELW product contains about 2000 IR winds.

4.4.2 Summary

The ELW product is based on cloud tracking in the IR channel. The ELW product is impacted by the difference noted in CLM product, where 20 % fewer cloudy pixels have been found on VAL. Consequently, as fewer pixels are identified as cloudy, the amount of ELWs extracted on the VAL chain is smaller than on the OPE chain.

Speeds and direction of collocated ELW extracted on OPE and VAL have, in general, good agreement. The density of the winds is taken into account for the calculation of the Pearson coefficients presented on the scatter plots in Figure 13 and Figure 14.

On average, wind pressures are found to be 30 hPa higher for VAL than for OPE. This means that GSICS-corrected ELW winds are located slightly higher in the troposphere. The pressure histograms of the two datasets are in relatively good agreement, despite some small differences at high and low levels. The pressures of collocated ELWs are in agreement at high levels, but the GSICS-corrected ELWs are found slightly lower in troposphere than their counterparts. This is because the height assignment of ELWs at low levels is mainly done using EBBTs, which are directly impacted by radiance correction. It can be noted that peaks related to low level temperature inversion areas are found in the same place in the pressure histograms seen in Figure 14.

4.4.3 Visualisation of the product

The top panel of Figure 13 shows examples of ELW product extracted from OPE (at left) and VAL (at right) on 19 October 2014 at 12:00 UTC. The middle panel shows the time series of the amount of ELW extracted during the studied period on OPE (black) and VAL (Red). The bottom panel shows the scatter plots of ELW directions (at left) and ELW speeds (at right) for collocated winds extracted over the whole period.

4.4.3.1 Analysis of ELW Height Assignment

The top panel in Figure 14 shows the time series of the average pressure of ELW extracted during the studied period on OPE (black) and VAL (red), while the lower panel shows the scatter plots of ELW pressure (at left) for collocated winds and the histograms of ELW pressure (at right) extracted over the whole period.

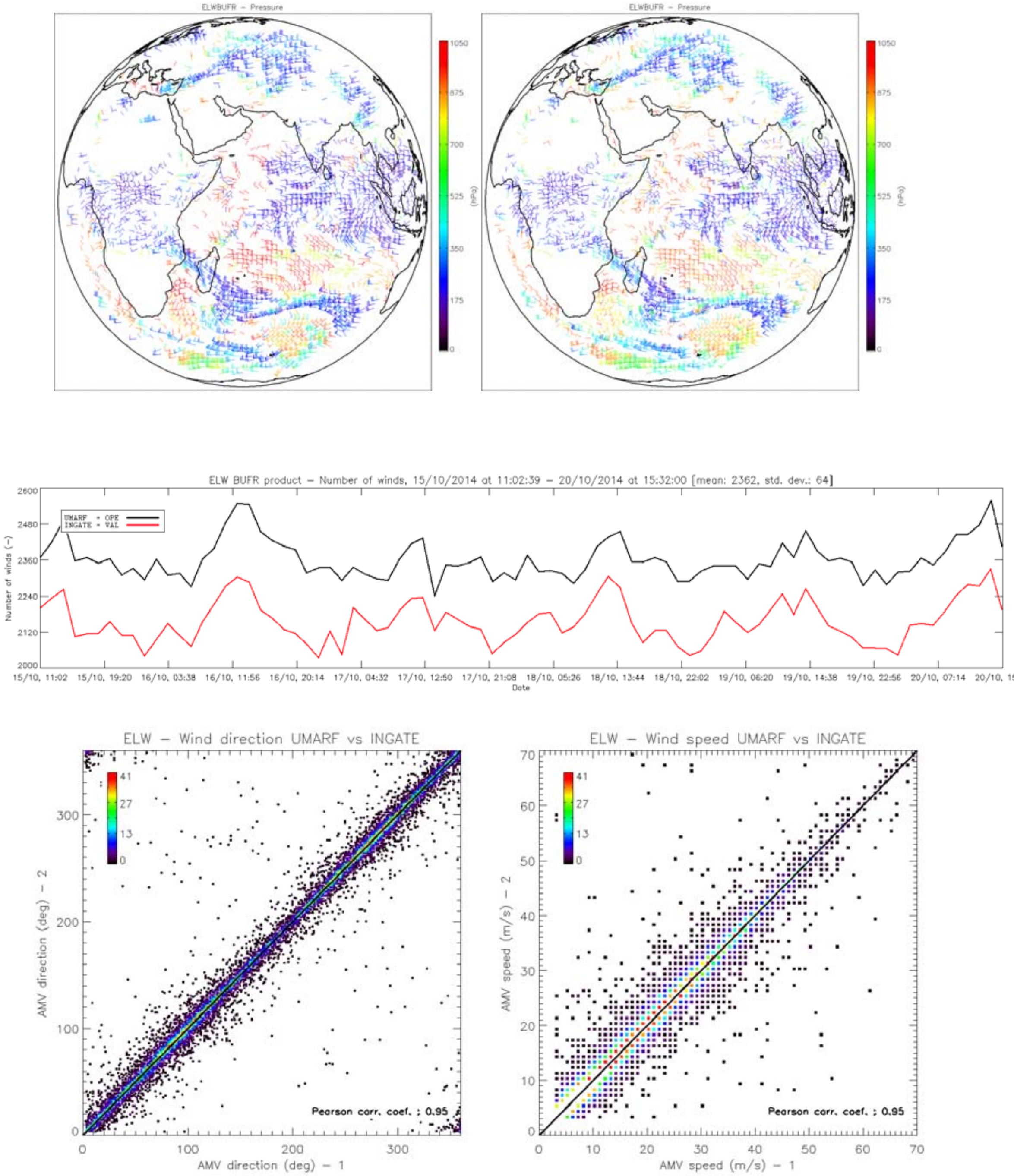

Figure 13: Example of ELW product extracted from OPE (upper left) and VAL (upper right) on 19 October 2014 at 12:00 UTC. The middle panel shows the time series of the amount of ELW extracted during the studied period on OPE (black) and VAL (red). Lower panels show the scatter plots of ELW directions and ELW speeds for collocated winds extracted over the entire period.

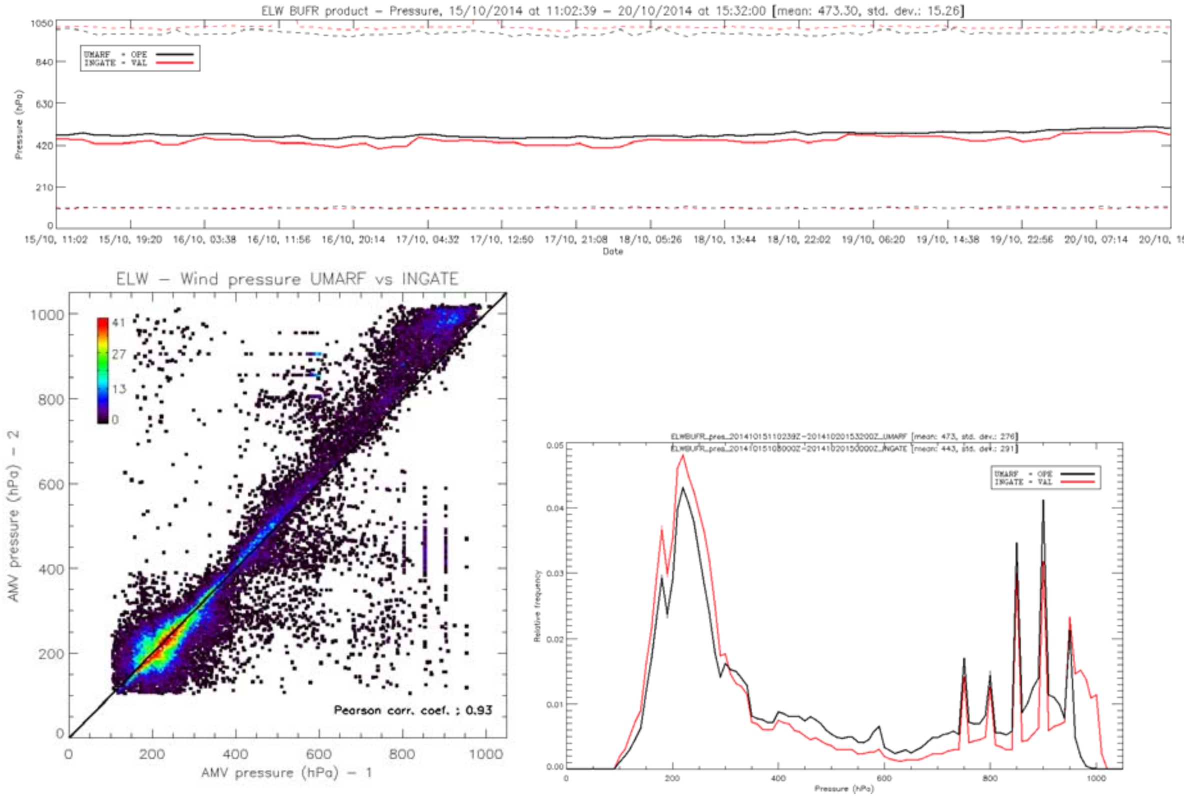

Figure 14: Top panel shows a time series of the average pressure of ELW extracted during the studied period on OPE (black) and VAL (Red). Lower panel graphs show the scatter plots of ELW pressure (left) for collocated winds and the histograms of ELW pressures (right) extracted over the whole period.

4.5 Comparison of High resolution Water Vapour Winds

4.5.1 Objective

Vectors are derived by tracking the motion of clouds using the Meteosat First Generation (MFG) WV channel. It uses a slightly different algorithm compared to the MFG IR vector product (ELW), namely the FFT surface correlation method. It uses the high resolution MFG matrix with 16 × 16 pixel segments, which is the same product resolution as the HRV product; but MFG WV image data is still low resolution. A typical HWW product contains about 5000 VW vectors.

4.5.2 Summary

The High Resolution Water Vapour Winds (HWW) product is also based on cloud tracking, but uses the water vapour channel. Like the ELW product, HWW is also impacted by the difference noted in CLM product. Therefore, the amount of HWW extracted on the VAL chain is also smaller than on the OPE chain. Generally, speeds and direction of collocated HWW extracted on OPE and VAL are in good agreement. On average, wind pressures extracted from OPE are found to be 17 hPa higher in the troposphere than those extracted from the VAL chain. The pressure histograms of the two datasets are in good agreement.

4.5.3 Visualisation of the product

The top panel in Figure 15 shows examples of HWW product extracted from OPE (at left) and VAL (at right) on 19 October 2014 at 11:00 UTC. The middle panel shows the time series of the amount of HWW extracted during the studied period on OPE (black) and VAL (red). The bottom panel shows the scatter plots of HWW directions (at left) and HWW speeds (at right) for collocated winds extracted over the whole period.

4.5.3.1 Analysis of HWV Height Assignment

The top panel in Figure 16 shows the time series of the average pressure of HWW extracted during the five-day period on OPE (black) and VAL (red). The bottom panel show the scatter plots of HWW pressure (at left) for collocated winds and the histograms of HWW pressure (at right) extracted over the entire five-day period.

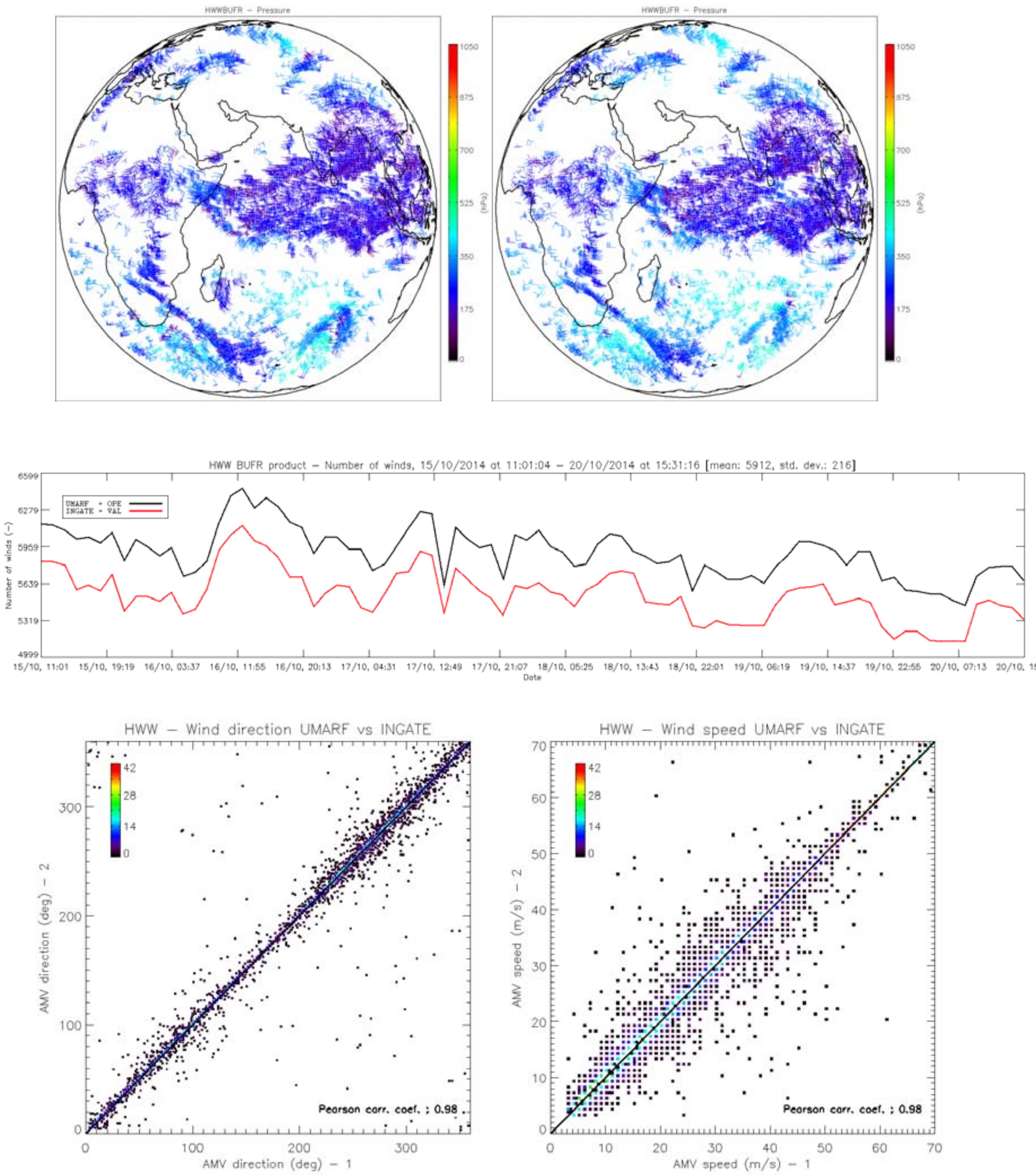

Figure 15: Example of HWW product extracted from OPE (upper left) and VAL (upper right) on 19 October 2014 at 11:00 UTC. Middle plot shows the time series of the amount of HWW extracted during the studied period on OPE (black) and VAL (Red). Lower graphs show respectively the scatter plots of HWW directions and HWW speeds for collocated winds extracted over the whole period.

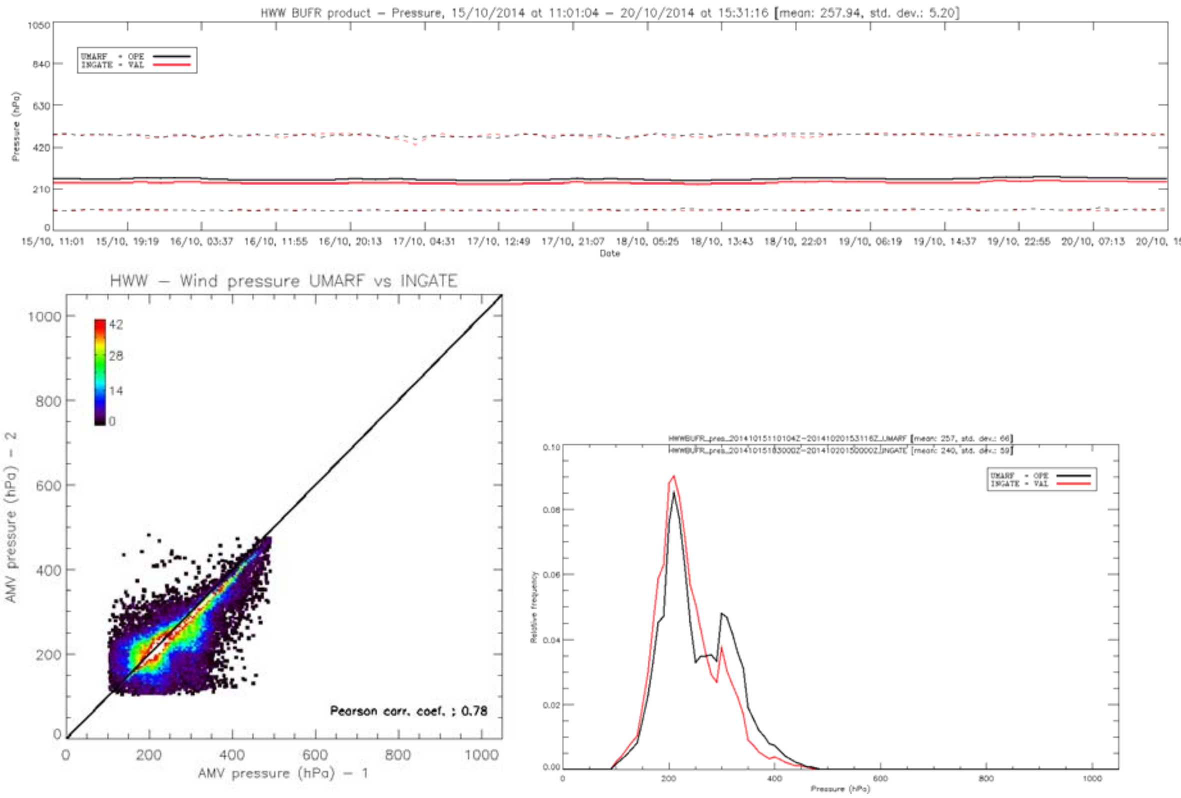

Figure 16: Time series of the average pressure of HVW extracted during the studied period on OPE (black) and VAL (red). Lower panel shows the scatter plots of HVW pressure (left) for collocated winds and the histograms of HVW pressure (right) extracted over the whole period.

4.6 Comparison of High Resolution Visible Winds (HRV)

4.6.1 Objective

High Resolution Visible Wind (HRV) vectors are derived using essentially the same algorithm as the ELW IR product; however, they are applied to the VIS images in full resolution and use the high resolution segment matrix with a 16 × 16 pixel segment size. A typical HRV product from daylight hours will contain up to 3000 vectors.

4.6.2 Summary

The HRV product is based on cloud tracking in the High Resolution Visible channel. However, despite the use of the CLM product for HRV extraction – similar to ELW and HWW products – the amount of HRV extracted on OPE and VAL are similar. This is because the HRV are only extracted at low levels where the cloud identification is more accurate than at high levels. Therefore, the impact of the cloud mask is smaller on HRV than on the two other products. Similar to the ELW and HWW products, the speeds and direction of collocated HRV extracted on OPE and VAL are generally in good agreement. On average, wind pressures are found on to be 19 hPa less for HRV extracted from OPE than from VAL, because GSICS-corrected HRV winds are located slightly lower in the troposphere. The pressure histograms of the two datasets and the pressures of collocated HRVs confirm this result, see Figure 18.

4.6.3 Visualisation of the product

The top panel in Figure 17 shows examples of HRV product extracted from OPE (at left) and VAL (at right) on 19 October 2014 at 8:00 UTC. The middle panel shows the time series of the amount of HRV extracted during the studied period on OPE (black) and VAL (red). The bottom panel shows the scatter plots of HRV directions (at left) and HRV speeds (at right) for collocated winds extracted over the whole five-day period.

4.6.3.1 Analysis of HRV Height Assignment

The top panel in Figure 18 shows the time series of the average pressure of HRV extracted during the five-day period on OPE (black) and VAL (red). The bottom panel shows scatter plots of HRV pressure (at left) for collocated winds and the histograms of HRV pressure (at right) extracted over the entire five-day period.

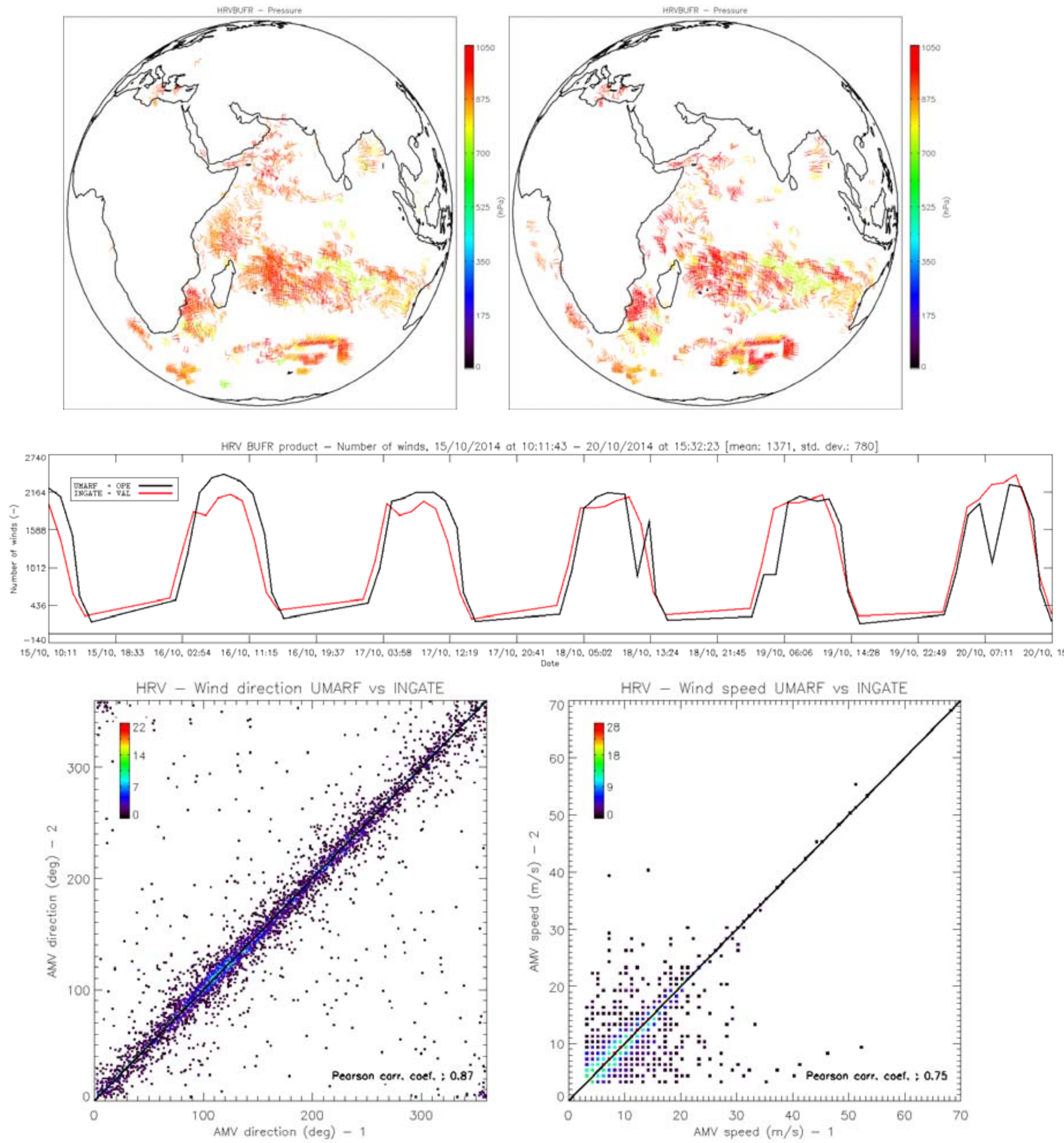

Figure 17: Example of HRV product extracted from OPE (upper left) and VAL (upper right) on 19 October 2014 at 8:00 UTC. The middle panel shows the time series of the amount of HRV extracted during the five-day period on OPE (black) and VAL (red). The bottom panel shows respectively the scatter plots of HRV directions and HRV speeds for collocated winds extracted over the entire period.

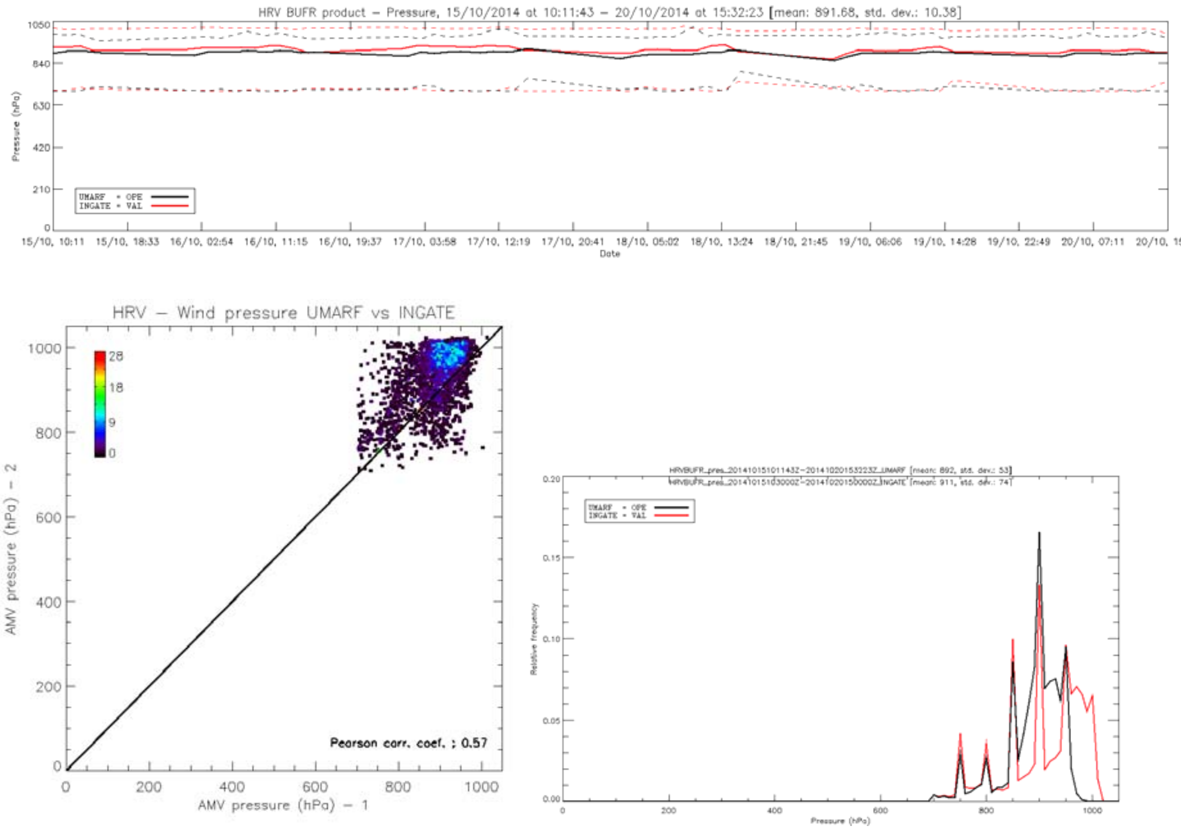

Figure 18: Time series of the average pressure of HRV extracted during the studied period on OPE (black) and VAL (red). The bottom panel shows the scatter plots of HRV pressure (at left) for collocated winds and the histograms of HRV pressure (at right) extracted over the whole period..

4.7 Comparison of Clear Sky Water Vapour Winds

4.7.1 Objective

The Clear Sky Water Vapour Winds (WVW) product uses essentially the same algorithm as the other wind products, but uses tracking structures in the WV image from non-cloudy areas. Additional height assignment information is supplied – the 10 %, 50 % and 90 % levels of the cumulative contribution function (based on ECMWF forecast data) – and the levels of the maximum gradient of the cumulative contribution function are inserted. These values allow characteristics of the layer being tracked to be determined. The values themselves are inserted in the fields designated for this purpose in the BUFR template. The product is generated every 1.5 hours and distributed in BUFR.

4.7.2 Summary

The WVW product is also based on water feature tracking in clear sky areas using the Water Vapour channel. The CLM product is used to identify clear sky targets. As there are fewer cloudy pixels identified on VAL, the amount of WVW extracted on the VAL chain is consequently larger than on the OPE chain. We can consider that HWW and WVW products are somewhat complementary. In this study, there were more HWW cloudy targets identified on OPE than on VAL, with opposite results for the WVW product. Speeds and direction of collocated WVW extracted on OPE and VAL are in good agreement like for other wind products. On average, wind pressures extracted from OPE are found to be 18 hPa lower in the troposphere than those extracted from the VAL chain. In Figure 20, the pressure histograms of the two datasets and the scatter plots of collocated WVWs show this small bias.

4.7.3 Visualisation of the product

The top panel in Figure 19 shows examples of WVW product extracted from OPE (at left) and VAL (at right) on 19 October 2014 at 11:00 UTC. The middle panel shows the time series of the amount of WVW extracted during the study period on OPE (black) and VAL (red). The bottom panel shows the scatter plots of WVW directions (at left) and WVW speeds (at right) for collocated winds extracted over the entire study.

4.7.3.1 Analysis of WVW Height Assignment

The top panel in Figure 20 shows the time series of the average pressure of WVW extracted during the five-day period on OPE (black) and VAL (red). The lower panel shows the scatter plots of WVW pressure (left) for collocated winds and the histograms of WVW pressure (right) extracted over the entire five-day period.

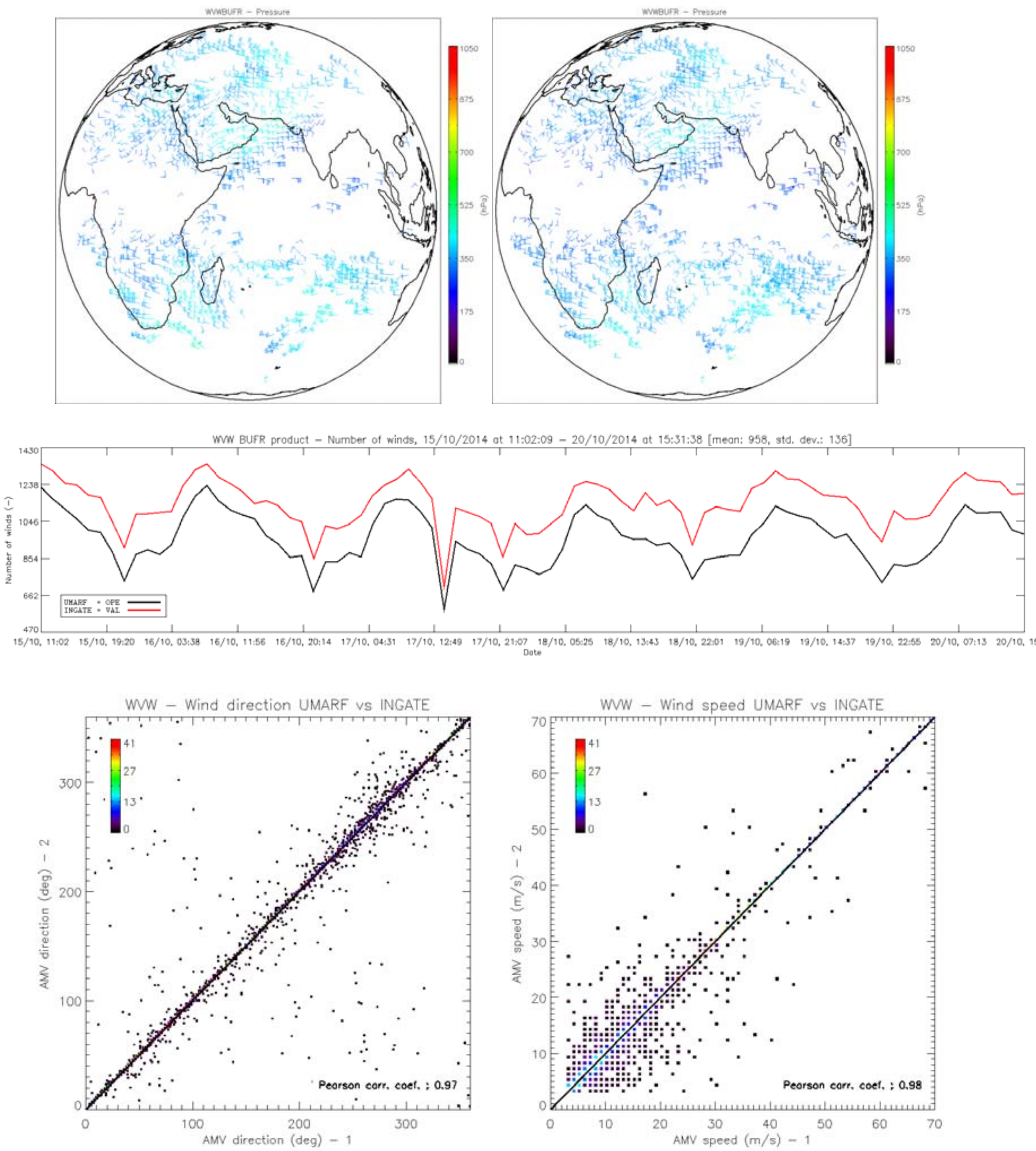

Figure 19: Example of WVW product extracted from OPE (upper left) and VAL (upper right) on 19 October 2014 at 11:00 UTC. The middle panel shows the time series of the amount of WVW extracted during the study period on OPE (black) and VAL (red). The lower panel shows the scatter plots of WVW directions and WVW speeds for collocated winds extracted over the entire study period.

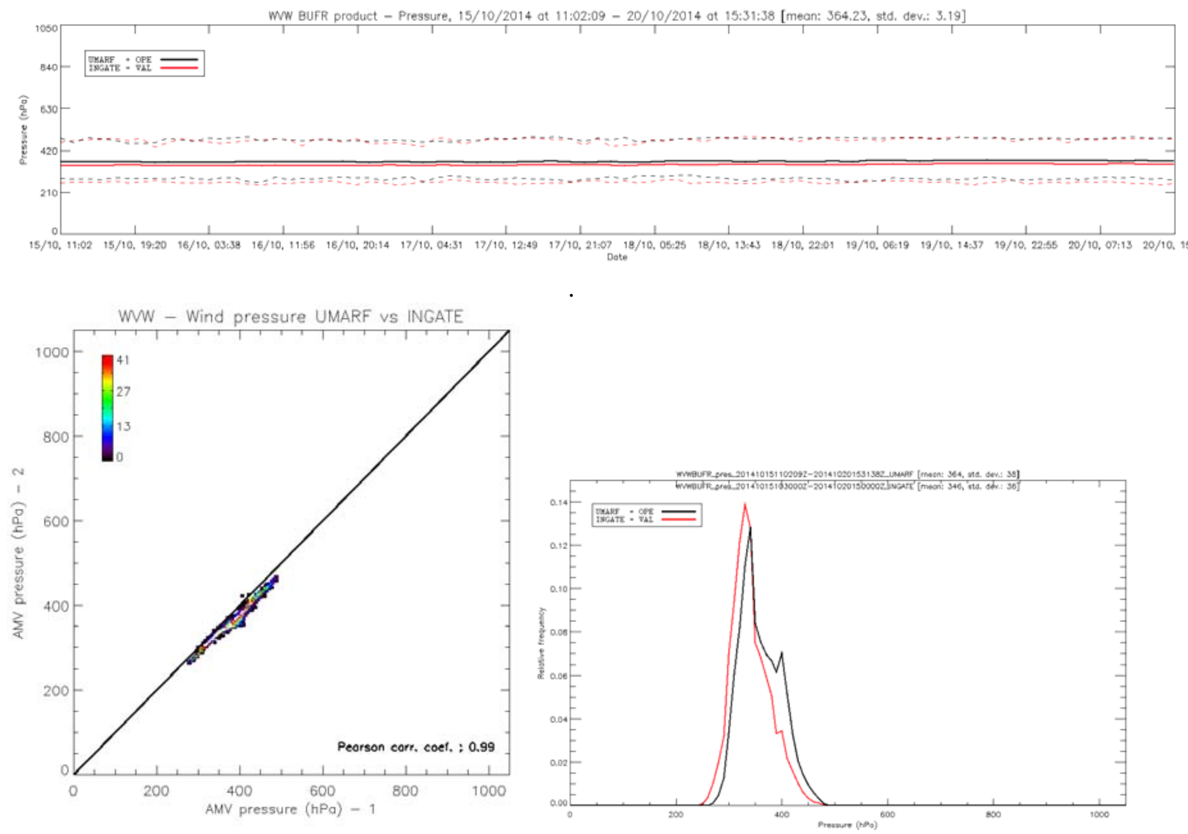

Figure 20: Time series of the average pressure of WVW extracted during the five-day period on OPE (black) and VAL (red). The bottom panel shows the scatter plots of WVW pressure (left) for collocated winds and the histograms of WVW pressure (right) extracted over the study period.

5 ADDITIONAL TESTS ON MFG WIND PRODUCTS

Additional small-scale tests have been done on the various AMV products extracted from the OPE and the VAL chain during the study period in order to get a more detailed estimate of the impact on product quality.

5.0 Impact of the diurnal cycle on AMV pressures

Average pressures for all AMV products extracted from OPE and VAL have been calculated within the range of six hours ranges including noon (from 09:00 to 14:59) and midnight (from 21:00 to 02:59) local time (UTC+4). Results of the average pressure differences (OPE - VAL) in hPa are presented in Table 1. Splitting the statistics as function of day/night has no impact on the average pressure difference between OPE and VAL, except for the ELW product. The most important difference occurs for the ELW product, for which the difference between OPE and VAL is around 21 hPa for the six hours range including noon, and nearly 45 hPa for the six-hour range including midnight. Obviously, there is no HRV product extracted during hours of darkness.

	day_6h	full	night_6h
ELW	21	30	45
HRV	-19	-19	-
HWW	18	17	19
WVW	18	18	19

Table 1: Average pressure differences between OPE and VAL in hPa for six-hour time periods spanning noon and midnight.

5.1 Statistics from Long Term Statistic database at EUMETSAT.

The long-term statistical database at EUMETSAT allows comparisons between OPE and VAL chain outputs for HRV and CMV wind products extracted from MFG. The CMW product is a high-quality subset of the ELW product. The winds are derived for all three spectral channels (VIS in half resolution) as well as for the ELW Product. The CMW product, however, only includes the best wind for each segment as determined from the QI value.

5.1.1 CMW product

Figure 21, Figure 22, and Figure 23 represent the OPE and VAL time series of several CMVs statistics obtained during the study period. The three panels in Figure 21 plot OPE in blue and VAL in red and show:

- Top panel: the total number of CMV extracted on OPE and VAL,
- Middle panel: the proportion of bad quality winds (where the quality indicator is less than 30),
- Bottom panel: the proportion of good quality winds (where quality indicator is more than 60).

As noted for ELW product in Section 4.3.2, the amount of winds extracted on VAL is smaller than for OPE. This is mainly due to the impact of the GSICS correction on the CLM product, which tends to reduce the amount of cloudy pixels by 20 % compared to OPE.
Figure 22 shows the corresponding vertical distribution of the CMV-averaged pressures. The panels show (in descending order):

- Top panel: vertical distribution of the CMV-averaged pressures split as low levels (below 700 hPa),
- Middle panel: vertical distribution of the CMV-averaged pressures split as mid levels (700 – 400 hPa),
- Bottom panel: vertical distribution of the CMV-averaged pressures split as high levels (below 400 hPa).

Note that the VAL chain has systematically extracted more CMVs at high levels than the OPE chain, and less CMVs at mid levels and low levels.

Figure 23 shows the following for the CMVs:

- Top panel: averaged vector consistency,
- Middle panel: averaged forecast consistency,
- Bottom panel: averaged quality Index (QI)

Note that the overall quality of CMVs is very similar on both VAL and OPE. However, it can be noted that the averaged forecast consistency is slightly worse on the VAL chain.

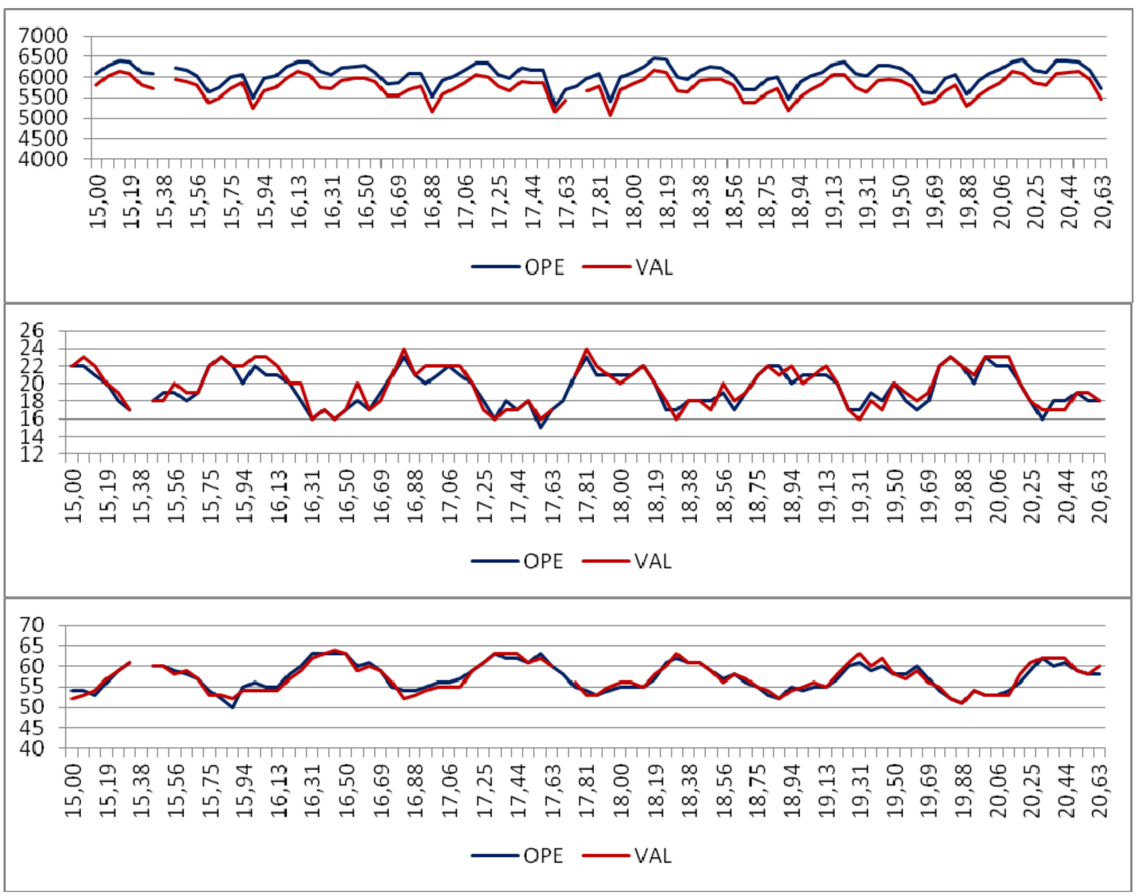

Figure 21: Time series of the total number of CMV extracted during the studied period on OPE (blue) and VAL (red), (top panel), the proportion of bad quality winds (middle panel) and the proportion of good quality winds (bottom panel).

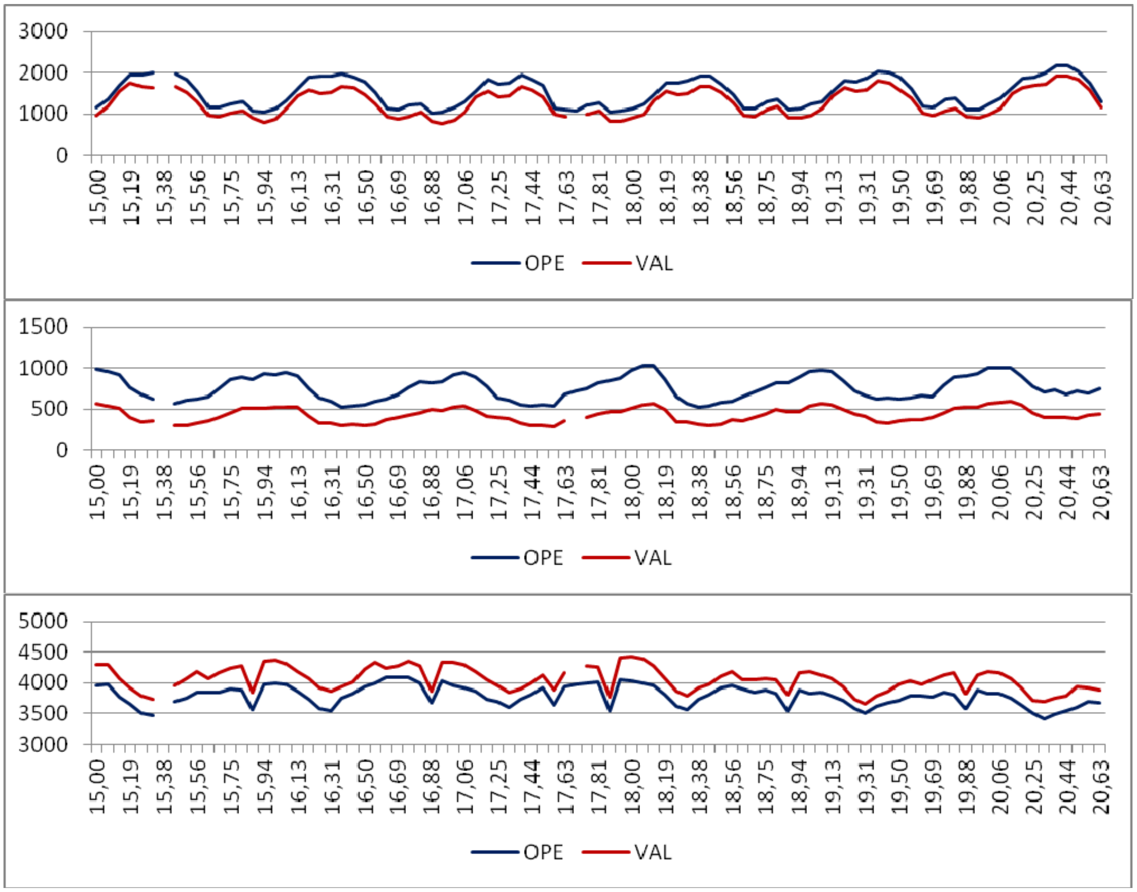

Figure 22: Corresponding time series of the total number of CMV extracted during the studied period on OPE (blue) and VAL (red). Upper, middle and lower panels correspond respectively to low-levels CMVs (below 700 hPa), middle-level CMVs (between 700 and 400 hPa) and high-level CMVs (above 400 hPa) .

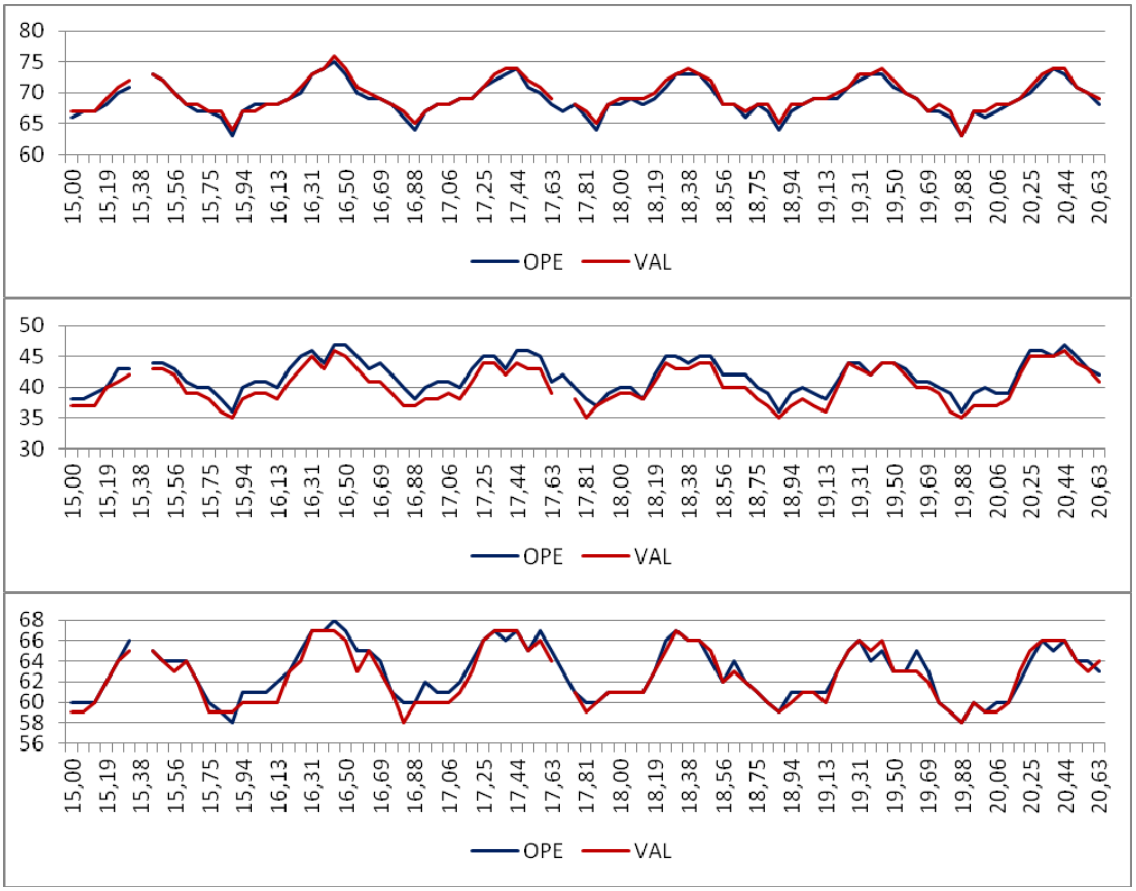

Figure 23: Corresponding statistics for the average vector consistency on OPE and VAL, (top panel), the average forecast consistency (middle panel) and average quality index (bottom panel).

5.1.2 HRV Product

Figure 24 and Figure 25 represent the same results as Figure 22 and Figure 23, respectively, but are applied to HRVs statistics obtained during the study period. The amount of HRVs extracted on VAL is a bit larger than for OPE, and the proportion of good winds (QI > 60) is also larger. Overall, the quality of HRVs appears to be better on VAL than on OPE.

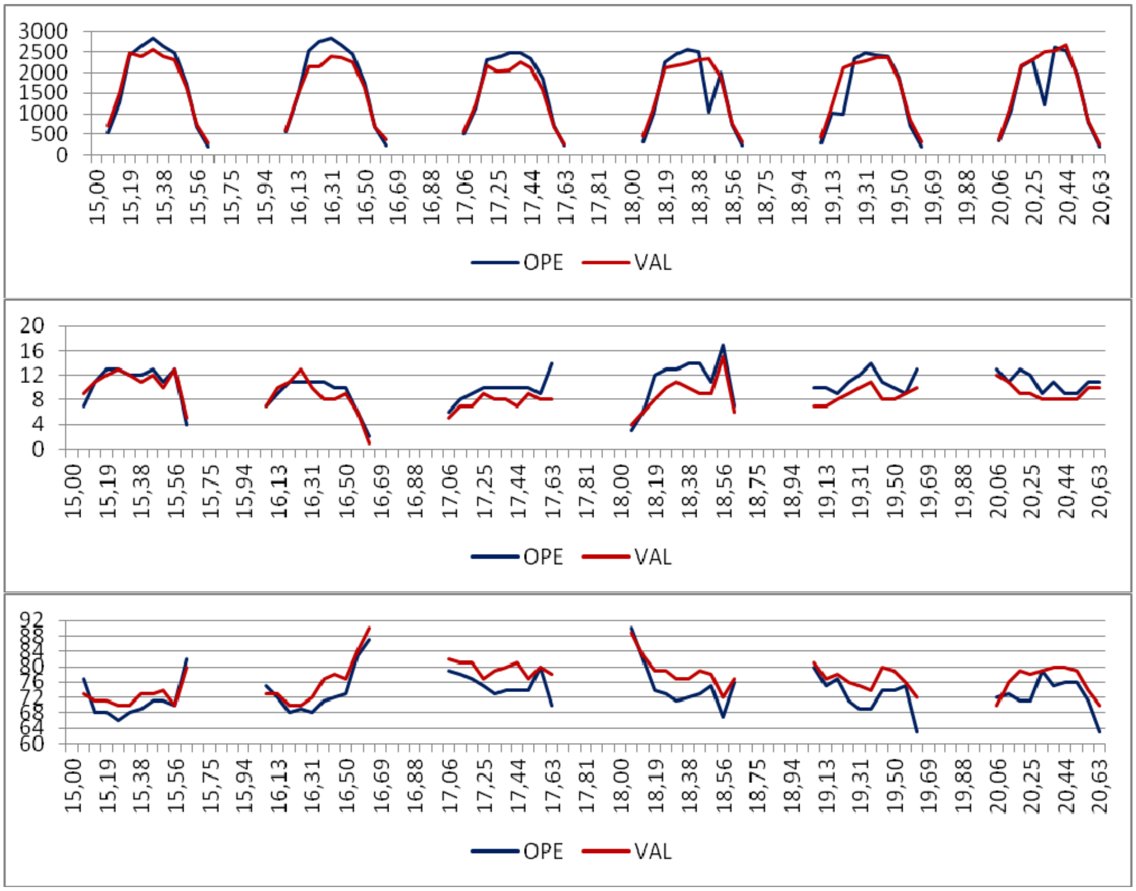

Figure 24: Time series of the total number of HRV extracted during the studied period on OPE (blue) and VAL (red), (top panel), the proportion of bad quality winds (middle panel) and the proportion of good quality winds (bottom pane).

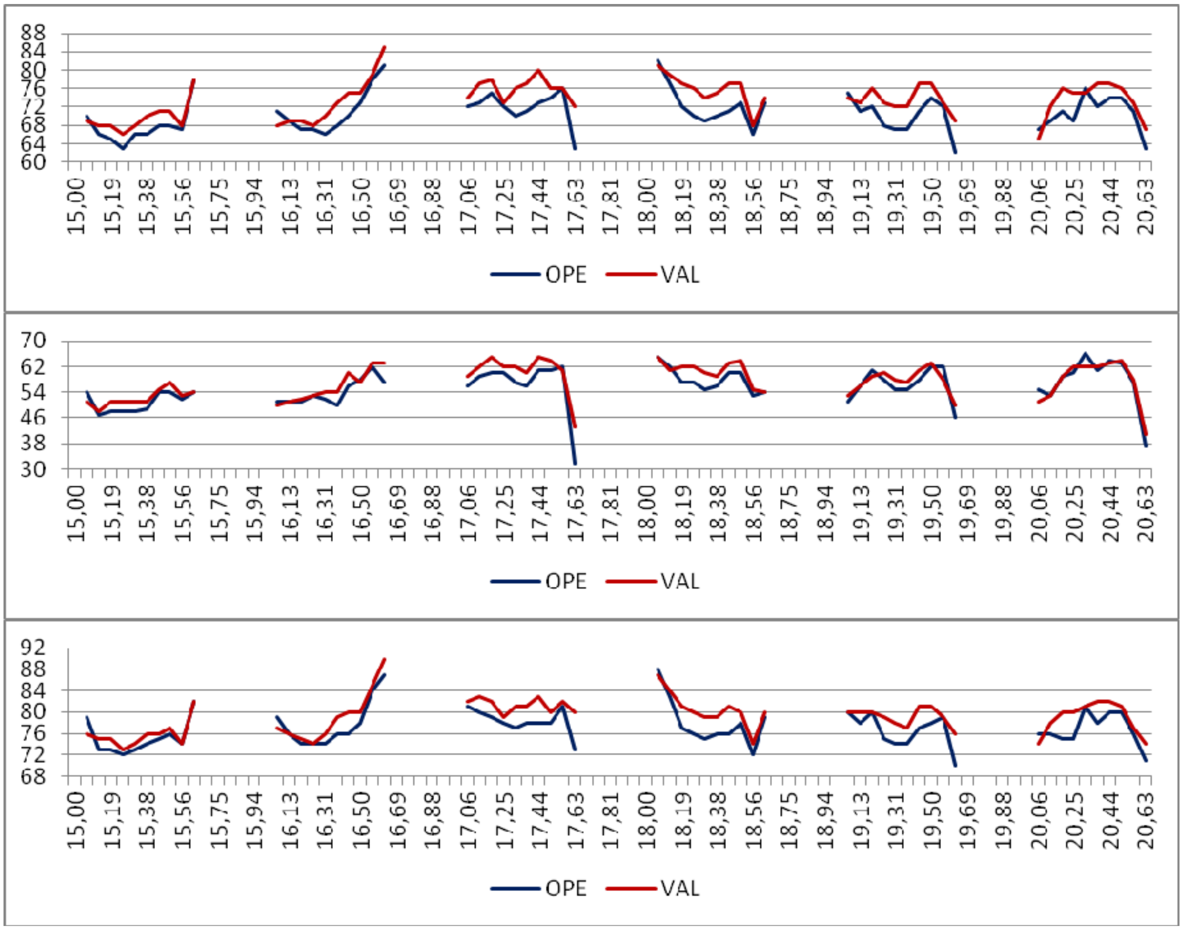

Figure 25: Corresponding statistics for the average vector consistency on OPE and VAL (top panel), the average forecast consistency (middle panel) and average quality index (bottom panel).

5.2 Inter-comparison of Metosat First Generation and Meteosat Second Generation

The present longitude locations of Meteosat 7 and Meteosat 10 satellites in orbit have a large overlapping area where the respective MFG and MSG winds products can be compared as shown in Figure 26.

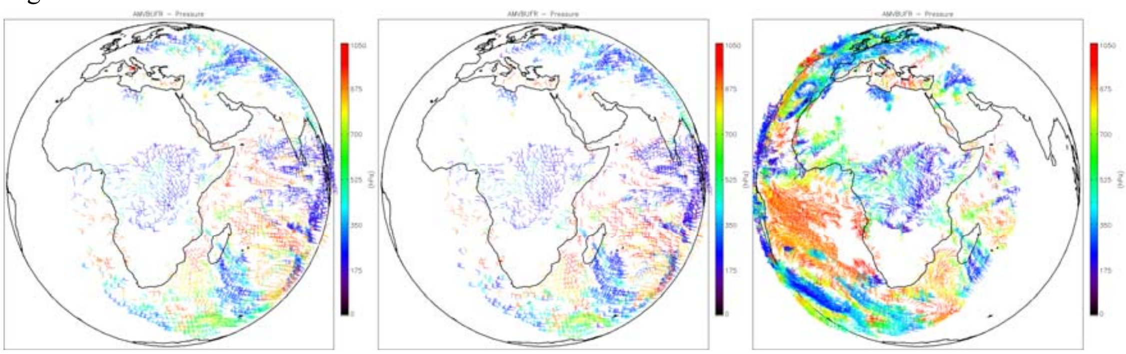

Figure 26: Illustration of the MFG and MSG overlapping area. The three graphics show the ELW product extracted from OPE (left), ELW product extracted from VAL (middle) and the corresponding MSG IR10.8 AMVs (right) extracted on 20 October 2014 at 7:45 UTC.

Collocations between MFG and MSG wind products have been obtained using 0.25 × 0.25 degree of latitude / longitude areas with products extracted within the same hour. Only the MFG and MSG winds having a QI larger than 60% have been considered for collocations.

In the figures that follow extracts from VAL and OPE are compared as follows:

- ELW products have been compared to the MSG IR 10.8 AMVs in Figure 27,
- HWW and WVW products have been compared to MSG WV 6.2 AMVs in Figure 28 and Figure 29,
- HRV product has been compared to the MSG Vis0.8 AMVs in Figure 30.

Separate panels in Figure 27 to Figure 30 present the scatter plots of speed (top panel), direction (middle panel) and pressure (bottom panel). The Pearson correlation coefficients allow a quick comparison of the agreement between MSG AMVs and the corresponding VAL (left side in each figure) and OPE (right side of each figure) of MFG products. The agreement of wind speeds and directions extracted from MFG and corresponding MSG AMV products is generally very good. It is a bit better for MFG products extracted from VAL than for OPE. The largest differences occur for the WVW product; however, the correlation coefficients are also poorer for this product. The agreement between MFG and MSG AMV pressures is generally a bit worse for VAL chain, except for the HRV product, but the Pearson correlation coefficients are also small; this means that the correlation is not very good for the pressures in any case, perhaps because height assignment methods used to set wind altitudes for MFG and MSG are quite different.

Since 2012, MSG AMVs altitudes have been set using the corresponding cloud product (CLA-CTH) while older height assignment methods included in the AMV software are still used for MFG. Several methods are used depending on the cloud mask and on cloud type of the target. In summary, it is quite difficult to understand where the differences come from without doing a deep study of the functions of the CLM, CLA and CLA-CTH products. Such analysis cannot be done using the dataset used in this study because any such analysis would also have to investigate the impact of GSICS correction on the intermediate cloudy products that are not saved on OPE, not just the impacts on final wind pressure.

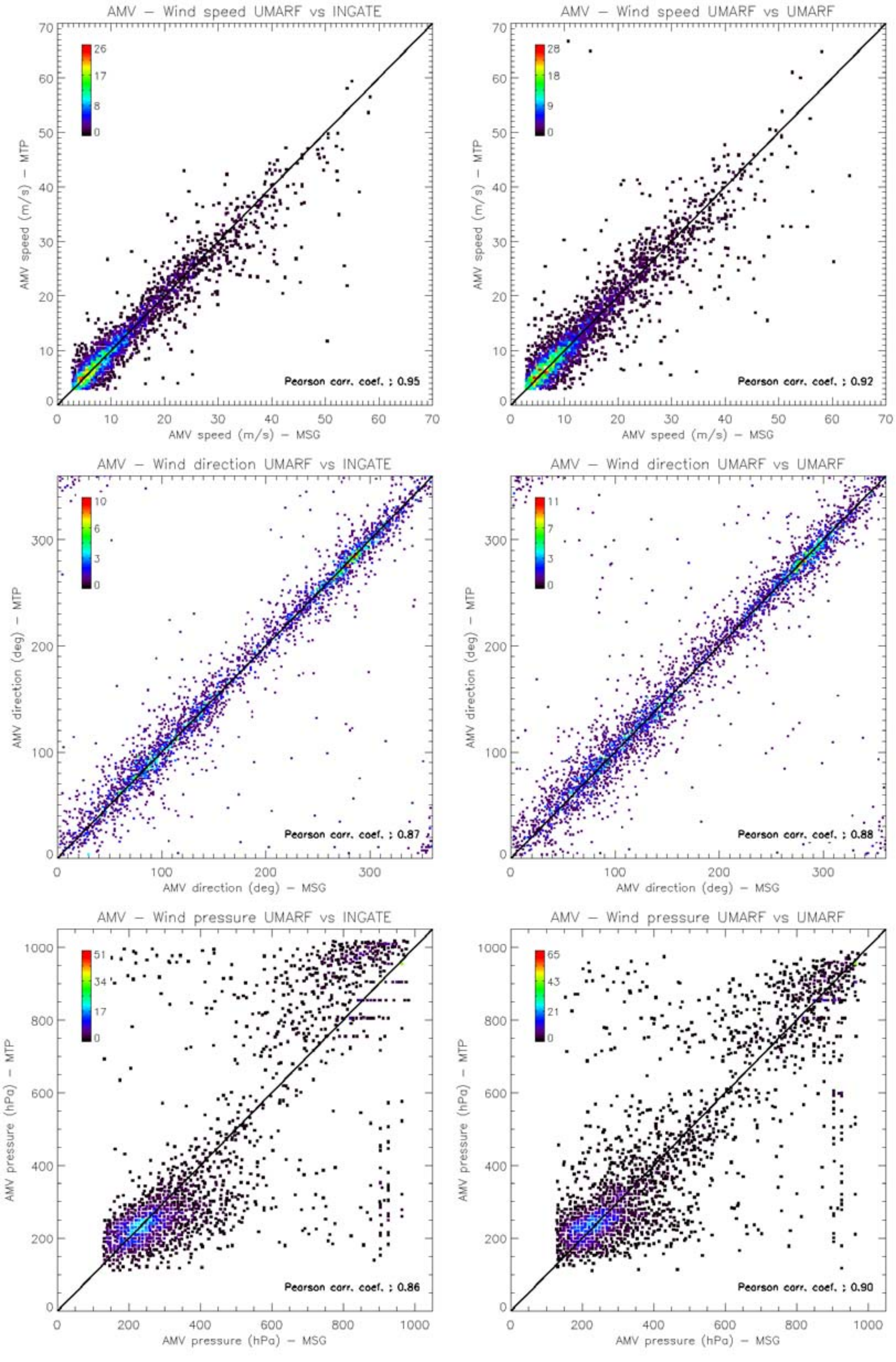

Figure 27: Inter-comparison of ELV winds extracted from VAL (left side) and OPE (right side) against corresponding MSG IR 10.8 AMVs for the study period.

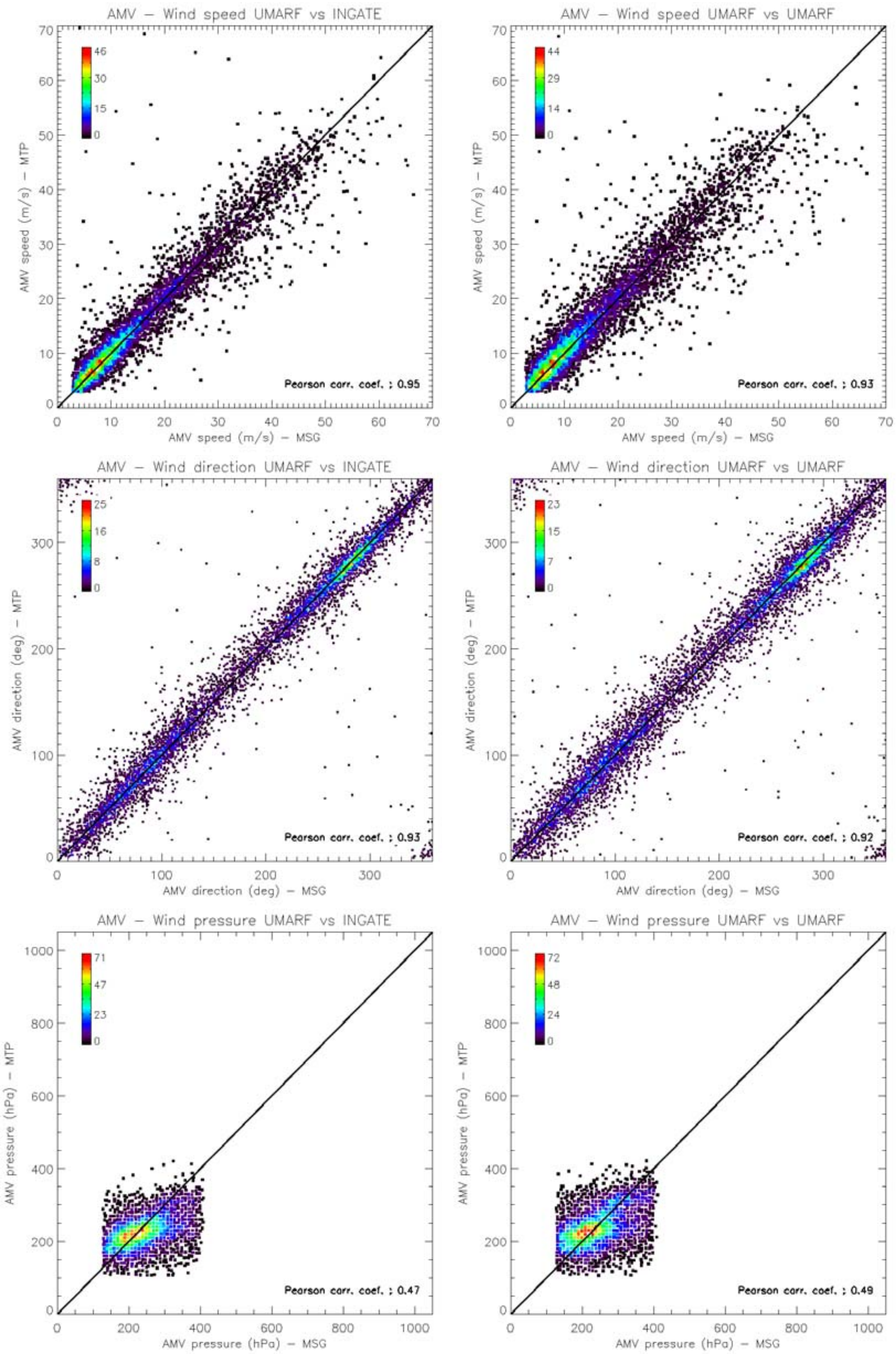

Figure 28: Inter-comparison of HWV winds extracted from VAL (left side) and OPE (right side)against corresponding MSG WV 6.2 AMVs for the study period.

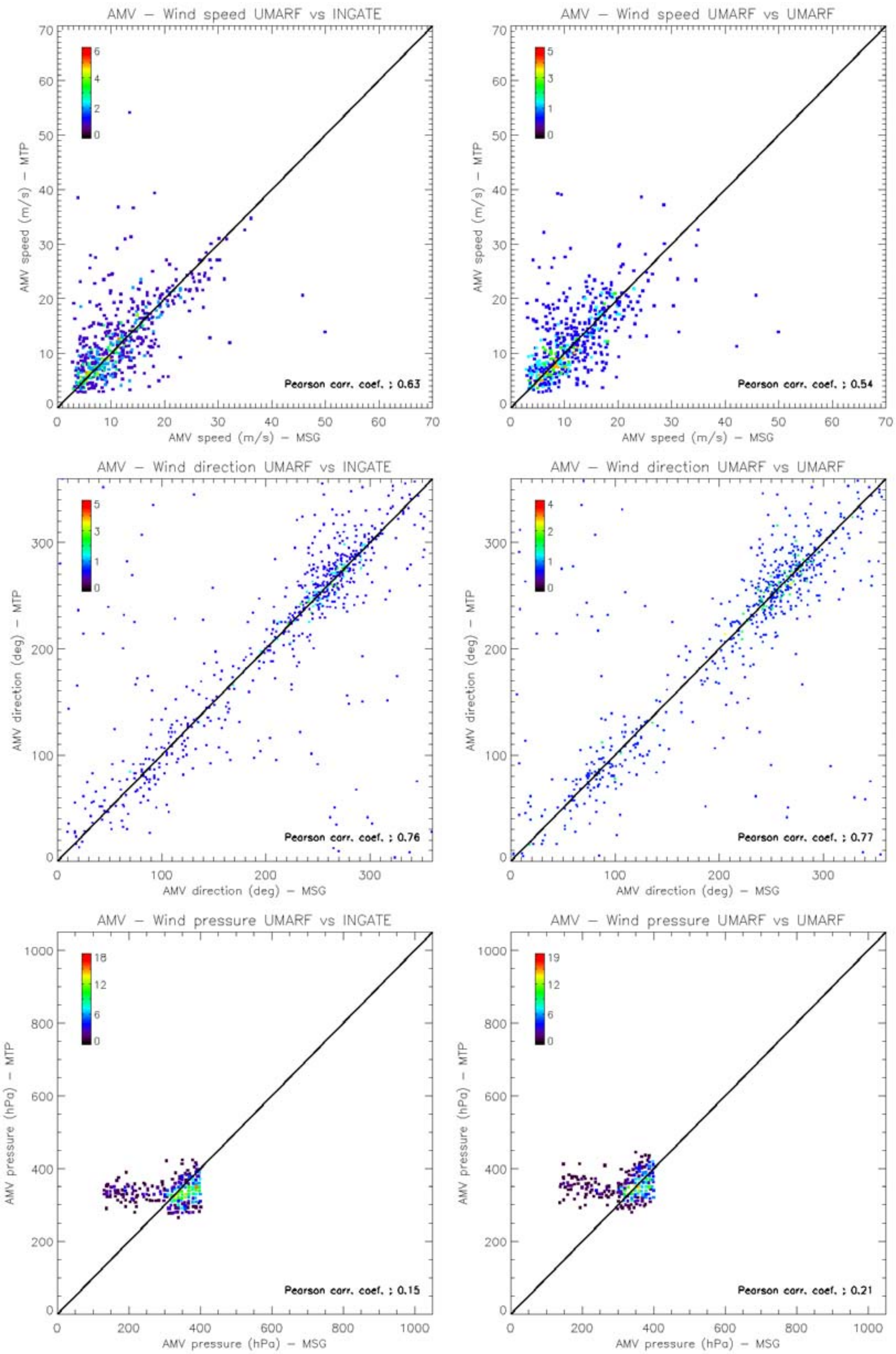

Figure 29: Inter-comparison of WVW winds extracted from VAL (left side) and OPE (right side) against corresponding MSG WV 6.2 AMVs for the study period.

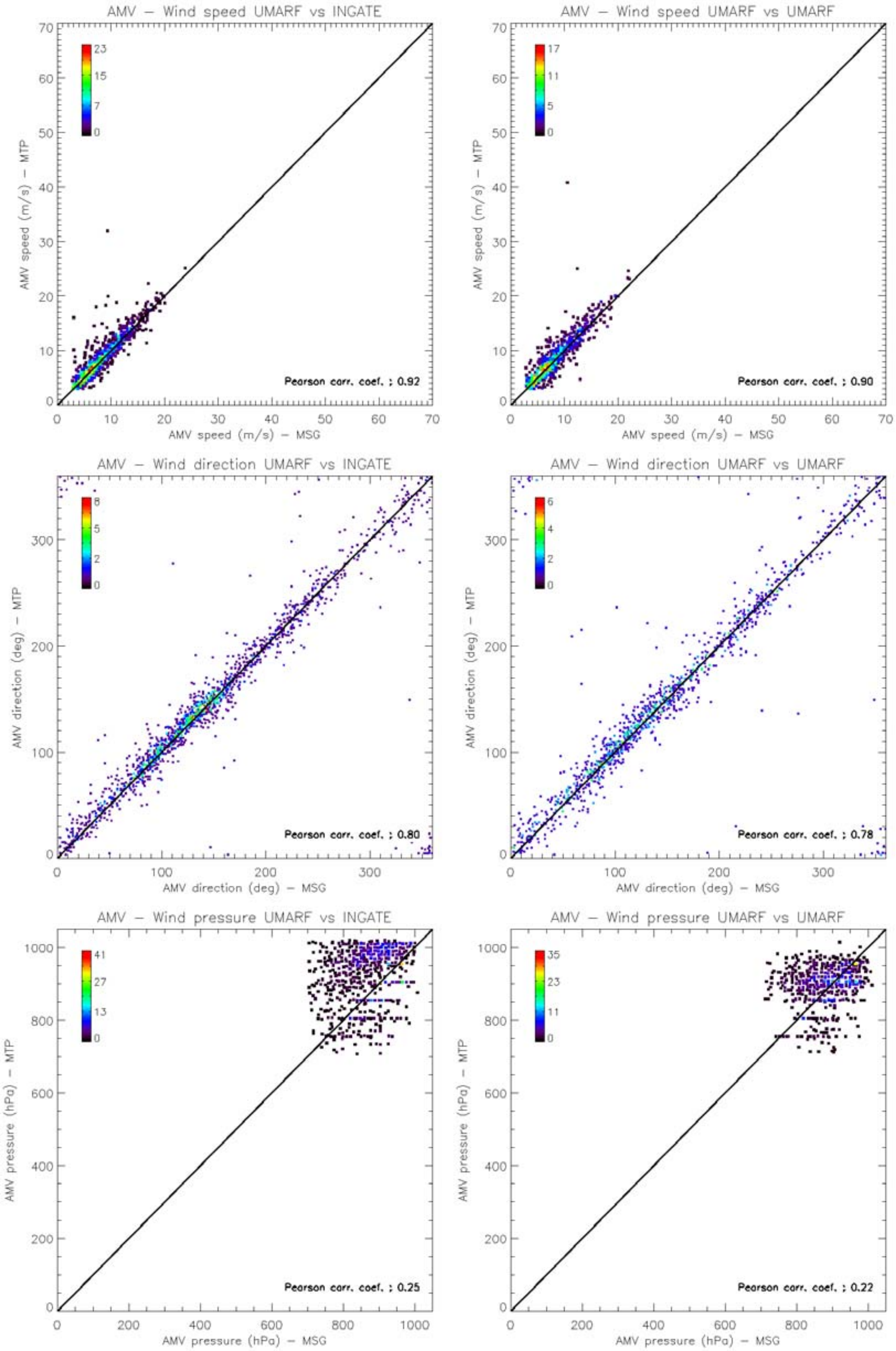

Figure 30: Inter-comparison of HRV winds extracted from VAL (left side) and OPE (right side) to corresponding MSG Vis 0.8 AMVs for the study period.

6 CONCLUSIONS

Despite the short time period studied in this report, the results clearly show that applying GSICS correction to the image radiance of MFG does have an impact on some of the meteorological products extracted operationally. Obviously, this is the case for the CSR product, which is directly estimated from the radiance.

This is also the case for CLM product, which is mainly based on thresholding methods. The number of cloudy pixels is reduced by 20 % when GSICS corrections are applied. This product is used as input in number of other algorithms like CSR, CLA, CTH and all the winds extraction algorithms. This 20 % difference on the CLM product impacts the calculations of the other products as well.

The results obtained on the winds are quite logical, showing a complementary split between clear sky and cloudy targets depending on the impact of the cloud mask on the wind products extraction. The wind speeds and directions are similar between the two datasets, but some important differences occur on the height assignment, which leads to different vertical distributions of the CMVs on the OPE and VAL chains. A quick check on the long-term statistic database shows a similar or slightly improved quality of the winds products when the GSICS corrections are applied. However, it must also be noted that despite the obvious scientific benefit of applying GSICS corrections, the correlation of winds products against FC fields are a bit worse on VAL in some cases. This explains the ambiguous conclusion of this section. A deeper analysis using independent datasets (radiosonde observations) is necessary to obtain a more objective and firm conclusion about the impact of GSICS corrections on the wind products quality. This type of study is far beyond the initial goal of this report and unfortunately cannot be done with the current datasets.

In conclusion, it is clear that applying GSICS corrections has an impact on the meteorological products extracted from MFG imagery. The impact is obviously more important on the products which are directly extracted using the images radiances like the CSR or the cloud mask, but the impact is also propagated to the products extracted at the end of the chain, like the CMVs. However, more profound studies that consider a longer period are needed to get a more objective and quantitative effects of the GSICS impact, especially on the cloud products (CLM, CLA, and CTH). Simple tests could be done by varying the thresholds used in the CLM algorithm for cloud identification, for example. However, an appropriate computing environment would be necessary to achieve this. This environment would allow us to reprocess the same dataset several times varying the setup parameters for each run. This flexibility did not exist in the operational environment used for the present study, and it constituted certainly an important limitation to a thorough investigation of the GSICS impact on MFG products. Such additional studies are necessary to better understand how to apply these corrections in the framework of future reprocessing activities.